Nanoscale control by chemically vapour-deposited polymers

Nanoscale Control with Chemically Vapor Deposited Polymers

Prof. Karen K. Gleason, Department of Chemical Engineering, MIT

Abstract

Chemical Vapor Deposition (CVD) brings nanoscale control to the characteristics of polymer thin films. Ultrathin (< 20 nm) and ultrasmooth (< 1 nm rms roughness) layers, as well as films > 10 μm thick, conform to the geometric structures on which the CVD polymers grow. Conformal coverage is essential for three-dimensional device architectures and electronics fabricated on papers and textiles. Systematic variation in CVD process parameters provides remarkable control of characteristics ranging π-π stacking distances and crystallite orientation in electrically conducting polymers, to mesh sizes in hydrogels. The CVD polymer processes scale to large areas and roll-to-roll processing and readily integrate with CVD processes widely utilized by the semiconductor industry for inorganic materials. CVD polymerization operates at low growth temperatures and allows for in situ grafting and single-step crosslinking to enhance durability. CVD polymers provide control over surface energy, permeation rates of molecules and ions, optoelectronic properties, and switchable smart behavior. These characteristics, combined with the low extrinsic defect densities of all-dry processing, enable novel approaches to energy storage and conversion, molecular separations, sensing and actuation, biotechnology, and catalysis. Fundamental understanding of CVD polymerization draws on the extensive knowledge base for both conventional polymers and CVD-grown inorganic thin films.

Introduction

Chemical Vapor Deposition (CVD) offers precision and purity for polymer layers.[1,2] In analogy to the inorganic CVD films widely employed in the semiconductor industry, polymers produced by CVD offer low defect densities, thickness control at the nanoscale, and ability to conformally cover complex nanostructures. In contrast, de-wetting and surface tension makes it challenging for solution-applied polymer processes to achieve pinhole-free ultrathin films and to retain the geometry of the underlying structure.

Rapid progress has resulted for CVD methods which preserve the fidelity of chemical structure of the monomer in the deposited film. The design of the different CVD methods relies on the mechanistic understanding of the multiple routes for macromolecule formation established by solution chemists.[3]

Step growth to form conjugated chains can be achieved by oxidative polymerization. When both the monomers and the oxidants arrive as vapors to the growth surface, the process is called oxidative CVD (oCVD, Fig. 1a).[4] The oxidant drives both polymerization and in situ doping. The sp^2 carbons in the backbone of the oCVD chains typically produces conjugation. The electrical and ionic conduction of oCVD thin films are of broad interest for optoelectronic and electrochemical applications.[5]

Chain growth occurs as a heterogeneous process involving the reaction absorbed monomers and an impinging volatile initiator (Fig. 1b).[6,7] The monomers for initiated CVD (iCVD) typically contain vinyl bonds (>C=C<) which polymerize to an all-sp^3 carbon backbone. Thus, the iCVD polymers are primarily dielectrics and span a range of surface energies, from superhydrophobic fluoropolymers to stable, highly-swellable hydrogels. Reactive organic moieties at the surface, allow post-deposition functionalization of iCVD surfaces with biomolecules and nanoparticles. The high density of organic functional groups in iCVD polymers can result in "smart" behavior in response to temperature, light, or pH. The capability of fine tuning the mesh size of crosslinked iCVD hydrogels enables selective permeation to molecules and ions differing in size and solubility characteristics.[8] Controlling diffusivity in thin organic layers underlies multiple applications including electrochemical energy storage, membrane separations, and controlled drug release.

Condensation polymers form by the reaction of pairs of organic functional groups. As a result of the coupling reaction, often an oxygen or nitrogen atom becomes part of the backbone, distinguishing condensation polymers from vinyl iCVD polymers. Alternation of the vapor flows of monomer pairs with allows the layer by layer growth, known as molecular layer deposition (MLD).[9,10] MLD shares many processing characteristics with Atomic Layer Deposition (ALD).

CVD paracyclophanes (i.e. parylenes) have a long history and have been widely commercialized as dielectrics. The library of CVD paracyclophanes continues to grow, providing an increasing diversity of organic functionalities, particularly for applications in biotechnology.[11,12]

This review will focus on the most recent developments for oCVD and iCVD polymers. Both methods operate at low growth temperatures and have been scaled up and demonstrated for roll-to-roll deposition.[13,14,15,16,17] While predominately used for inorganic layers, hybrid materials have also been synthesized by both oCVD and iCVD. Details on the progress achieved for other CVD polymer methods can be found in the reviews cited above.

oxidative Chemical Vapor Deposition (oCVD)

Synthesis Strategies

Monomers for oCVD include thiophene, aniline, pyrrole, selenophene, and their derivatives[5,18]. Additional oCVD monomers are metal porphyrins[19]; and dopamine[20].

Oxidant vapors can be produced by the sublimation of a solid such as $FeCl_3$, $CuCl_2$, or $MoCl_5$. [21,22] More volatile oxidants include the liquids $VOCl_3$, $SbCl_5$, H_2SO_4; and Br_2 gas. [23,24,25,26] Volatile oxidants can eliminate the need for post-deposition rinsing and thus allow oCVD to be single-step all-dry process. If the flows of oxidant and monomer are alternated, the technique is termed oxidative MLD (oMLD).[22]

Grafting improves interfacial adhesion to the substrate. Delamination failures are reduced, particularly during pattern formation steps used to create devices. For *in situ* linker-free grafting, oxidant vapor exposure causes a Friedel-Crafts reaction directly on surfaces possessing aromatic groups (Fig. 1c).[27] Such substrates includes the flexible organic films polyethylene terephlate (PET) and polyethylene naphthalate (PEN). The resulting radical cation is surface site for the

growth of grafted oCVD chains. Alternatively, *ex situ* grafting for oCVD proceeds by pretreatment of the growth surface with a linker molecule, such as phenyl trichlorosilane[27], vinyl trichlorosilane[28, 29], or decadiene[30].

Optoelectronic and Thermal Properties and Devices

The intensive interest in conducting polymers derives from their electrical, optical, and thermal properties combined with their mechanical flexibilty. [31,32,33] Additionally, the conformal nature of oCVD enables integration of conducting polymers into three-dimensional hybrid organic/inorganic device architectures[34] and into electronics fabricated directly on papers and textiles[35,36].

The monomer 3,4-ethylene dioxythiophene (EDOT) produces oCVD PEDOT thin films which can exhibit electrical conductivity, σ, > 6000 S/cm, [37] exceeding the of all previously reported methods.[38] The maximum σ values fall in the range for indium tin oxide (ITO).[39] ITO is widely utilized as transparent conductor, but has limited mechanical flexibility as compared to organic polymers.

The choice of oxidant determines the small anionic dopant species, chlorine, bromine, or sulfate ions, in the as-deposited film. The oxidant strength and concentration influences chain length and macroscopic growth rate. High conductivity also requires significant conjugation length along the polymers chain and maintaining the fidelity of chemical structure of the EDOT monomeric unit. The loss of full chemical functionality and conjugation by plasma vapor deposition methods substantially reduces σ to ~10^{-2} S/cm.[40] PEDOT films produced from solution display significant loss in σ with decreased measurement temperature, reflecting higher levels of intrinsic disorder than is present in oCVD layers.[25] Increasing σ correlates with reduced oCVD PEDOT disorder, as revealed by optical determined Urbach edge width.[33]

The oCVD synthesis approach provides systematic control over crystallite sizes (< 1 nm to ~80 nm) in highly conducting semicrystalline PEDOT films (Fig. 2a).[29,41,42] Film thickness on the order of the crystallite dimensions can lead to 2D carrier transport with enhanced in-plane conductivity, $\sigma_{||}$.[29]

Preferential orientation of the oCVD PEDOT crystallites with respect to the growth surfaces produces anisotropic conductivity.[37] Texture can result from grafting[29], controlling growth temperature and film thickness[37], and from the choice of oxidant[33] In the face-on orientation, the extended states resulting from the π orbitals of the conjugated ring structures are parallel to the surface (Fig. 2b). The orthogonal orientation is known as edge-on texture. Face-on orientation typically requires the growth temperature to exceed the glass transition temperature, T_g, for PEDOT (~102 °C).[43] This observation suggests that molecular reorientation during film growth contributes to achieving face-on texture.

The face-on orientation produces significantly improved $\sigma_{||}$ (Fig. 2c).[37] For each oCVD PEDOT film represented in Fig. 2c, the Seebeek coefficient is 11 ± 1 μV/K and the work function is 5.33 ± 0.04 eV. Thus, any variations in p, the carrier concentration, are relatively modest. Therefore,

the observed changes in $\sigma_{||}$ must result primarily from the carrier mobility, μ. The maximum μ of 18.45 cm^2/Vs was measured using the Hall effect and is in agreement with values calculated using the Kang-Schneider model.

For the films represented in Fig. 2c, the energy barrier for intercrystalline charge transport was significantly higher in the edge-on orientation (175.4 meV) as compared to the face-on orientation (0.2 meV). [37] In the face-on orientation, there is a higher probability of having two adjacent crystallites with the same alignment (Fig. 2b), denoted as tilt angle of zero. In analogy, to transport in polycrystalline inorganic films[44], a zero tilt angle is hypothesized to facilitate intercrystallite charge transport in semicrystalline PEDOT, consistent with the low activation barrier determined for the face-on orientation.

Mechanisms for charge transport between PEDOT crystallites can occur in parallel. One hypothesis is course-grain variable range hopping (VHR).[29] The temperature dependent σ for oCVD PEDOT films follow the model predictions of a linear combination of Mott VHR with Efros-Shklovskii (ES) VHR. Mott's model assumes negligible interactions between delocalized electrons. The interactions assumed by the ES model opens up a soft Coulomb gap.

In parallel to VHR, conduction in along bridging chains has been hypothesized in highly-conductive oCVD PEDOT (Fig. 3a).[33] In the face-on orientation, adjacent crystallites have an increased probability of having the same orientation to form a percolation pathway and thus may create quasi-1D conduction (Fig. 3b). PEDOT chains which connect between regions of ordered π- π stacking are predicted by molecular dynamics simulations.[45] The presence of tie chains between ordered domains, has also been postulated to explain carrier transport in conjugated polymer poly(3-hexylthiophene), P3HT.[46,47] The synthesis method must achieve chains of sufficient molecular weight to create tie-chains, but further increases in molecular weight may not push σ higher.

For face-on oriented PEDOT, the improved transport between crystallites can render the transport within the crystallites as the overall the rate limiting step for σ.[33] Inside the ordered domains, the charge transport between adjacent chains is hypothesized to be rate limiting step, given by interchain charge transfer integral, ($t_\perp$),

$$t_\perp = t_0 \exp(-\gamma x), \quad (1)$$

where, t_o is the value at minimum distance , $1/\gamma$ is the wavefunction overlap decay length, and x is the π- π stacking distance.[33] Systematic variation of the oxidant vapor concentration, produced monotonic changes in the b-axis lattice parameter, which is the direction for π- π stacking.[33] Consistent with the hypothesis of chain-chain charge transport (Eq. 1) being the rate limiting step, σ increases as the b-axis lattice parameter decreases (Fig. 3c). Increasing $t_\perp$ was also postulated to contribute to the observed increase in σ for oCVD PEDOT upon applying a hydrostatic pressure (Fig. 3d).[41]

The trade-off between p and μ for two oCVD PEDOT films is shown in Fig. 3e.[48] The maximum p, 5.4 $x10^{21}/cm^3$, corresponds to ~90% ionization of monomer units. Higher levels of ionic dopants are hypothesized to increase scattering, hence lower μ. In strong support of this

hypothesis, the μ calculated by Brook-Herring-Dingle (BHD) theory matches to the values experimentally determined by Hall Effect measurements at ambient temperature.[49] The BHD theory is also utilized for inorganic transparent conducting oxides.[39] Because of the trade-off between p and μ, higher doping levels do not always correspond to higher overall conductivity.

The semiempirical understanding of conjugated polymers describes charge transport by polarons and bipolarons which are partially delocalized over the span of several monomer units.[50] In contrast, in traditional band conduction theory, charge transport occurs through fully delocalized states. For band theory[51], W<0 signifies metallic conduction, where the logarithmic temperature coefficient, W, is given by

$$W = d \ln \sigma / d \ln T. \quad \text{(Eq. 2).}$$

Alternatively, W<0 can be interpreted as hopping conduction in a Guassian Disorder Model which includes a temperature-dependent bimodal distribution of $t_{\perp}$ for PEDOT.[52]

Values of W < 0 been measured at low temperatures for highly conductive oCVD PEDOT films[41], including those displaying edge-on and face-on texture.[37] The face-on orientation yields the most negative values. Under conditions where W<0 , applying a 9T magnetic field increases σ, confirming a disruption in the delocalized carrier transport.[25] For W>0 in band theory, having σ proportional to $T^{0.25}$ is characteristic of an Anderson insulator. The proportionality of σ to $T^{0.25}$ has observed over some temperature ranges for oCVD PEDOT[41] and for oCVD polythiophene[53].

Electrochemical Behavior, Devices, and Processes

As a result of its small anionic dopants, oCVD PEDOT displays electrochemical behavior distinct from solution-applied PEDOT:PSS (Fig. 4).[43] The macromolecular dopant PSS has low mobility and yields corresponding low electrochemical activity. In contrast, the oCVD PEDOT films doped with Cl^- displays a large electrochemical window vs. Li/Li+. Edge-on texture with respect to the substrate improves charge storage capacity and electrochemical cycling rates as compared to the face-on texture.[43,54]

The oCVD PEDOT can also display superior electrochemical performance relative to PEDOT produce by Vapor Phase Polymerization (VPP).[55] While both oCVD and VPP use vapor phase monomers, only the oCVD method continuously supplies the oxidant as a vapor simultaneously with the monomer, allowing a constant ratio of monomer to oxidant to be maintained at the growth surface over the course of the deposition. In contrast, for VPP, a solid oxidant is first preapplied to the substrate, which is then exposed to monomer vapors, making control over the monomer to oxidant ratio at the growth surface more challenging.[56]

The cycling stability of lithium transition metal oxide battery cathodes improves upon conformal encapsulation by an ultrathin (~20 nm) of oCVD PEDOT (Fig. 3D). [57,58] The PEDOT can facilitate Li+ ion transport, form interfacial bonds with the metal oxide, suppress undesired phase transformation, and mitigate mechanical cracking.

Supercapacitors require optimized electrode design for increased energy density, faster charging/discharging rates, and long term cycling stabilty. Thus, the theoretical limit for energy storage is one electronic charge per monomer unit, favoring monomer units of low molecular weight. Indeed, the small oCVD thiophene[59] and aniline[24] have been exploited for supercapacitor research. Other characteristics, such as faster electrochemical kinetics or a larger electrochemical window, may favor selecting higher molecular weight monomeric units, such as 3-methyl thiophene[60] and EDOT[61].

Minimizing ion transport limitations requires avoiding the thick layers typically produced by solution-based processes. In contrast, ultrathin and systematically controlled oCVD PEDOT of 3 6, and 10 nm thicknesses provide ready integration into supercapacitors.[62]

Conformal oCVD layers over nanoporous materials can enhance their electrochemical performance and mechanical stablity.[5] While solution-applied layers may fail to wet or occlude pores, the nanoscale and conformal oCVD layers fully cover the interface with their porous substrate and leave the pore space open. Maintaining high surface allows effective contact by the electrolyte, as desired for improved cycling rates. For improved stability under long term cycling, the open pore spaces offers a means of relieving the mechanical strain resulting from the expansion and contraction induced by doping and dedoping.

Conformal coating with ~5 nm of oCVD poly(3-methyl thiophene) improved the areal capacitance of horizontally-aligned CNTs (HACNTs) electrodes by ~3x. The hybrid oCVD/HACNT electrodes displayed an areal capacitance of 9x that of unmodified CNT buckypaper and retained 92% of their stored charge stored after 5000 bends over a 5 mm radius of curvature. Flexibility is desired for wearable devices and producing energy storage in shapes that seamless integrate into final products.

As compared to unmodified carbide-derived-carbon nanoporous electrodes, oCVD polyaniline layers ~1.7 nm thick increased gravimetric capacity >2x at cycling rates up to 500 mV/s.[63] The oCVD PANI-modified electrodes retained 79% of their capacitance after 10,000 cycles. Some oCVD conditions produced porous PANI layers which displayed electrical double layer capacitance storage in addition to the pseudocapacitive mechanism.

Low temperature oCVD processing enabled fabrication of flexible supercapacitors on paper and on polymeric membranes. To achieve monolithlic integration, partially conformal oCVD PEDOT layers were grown on both faces of a porous substrate.[64] This approach eliminates the possibility of multilayer delamination and minimizes the weight and volume of inactive materials.

Using oCVD PEDOT, novel supercapacitors were fabricated directly on microstructured plant leaves and flower petals.[65] The oCVD of poly(3,4-propylenedioxythiophene) directly on living plant tissue resulted in electrodes used for detection of plant dehydration.[66]

Scalable metal-free catalysts are desired for sustainable processing. Oxygen reduction was achieved using ~40 nm oCVD PEDOT conformal applied to carbon cloth electrodes. [67] The highest electroactivity resulted for most conductive oCVD layers (σ > 2000 S/cm). Taking

inspiration from enzymatic reactions, carbon dioxide reduction was demonstrated using oCVD from dopamine.[20]

The room temperature thermal conductivity of oCVD PEDOT, 0.16 W/mK, falls below that of PEDOT:PSS.[68] Thus, oCVD PEDOT combines low thermal conductivity with high electrical conductivity. The maximum thermal conductivity achieved for oCVD poly(2-hexylthiophene). of 2.2 W/mK, a value is ~10x that of conventional polymers.[42]

intiated Chemical Vapor Deposition (iCVD)

Synthesis strategies

For iCVD, monomer and initiator vapors mix.[1,2] The use of an initiator is a mechanistically based distinction from methods using only monomer vapors. Typically, iCVD uses a free-radical initiator, such as tert-butyl peroxide (TBPO). However, cationic initiation[69,70], photo initiation[71,72], or low-power plasma initiation[73,74] are alternative CVD approaches.

For TBPO, resistively heated wires in the vacuum chamber cause thermal decomposition of the initiator vapors. For filament temperatures < 300 °C, tert-butoxy radicals are the predominate free radical species formed. At high filament tempertures, the tert-butoxy further decomposes to methyl radicals. The later species can be utilized for *in situ* grafting (Fig. 1d).

The relatively modest filament temperatures produce little if any decomposition of the monomers. Cooling of the growth stage promotes adsorption of the monomers as required for heterogeneous polymerization. Typical stage temperatures are between ~25 and ~65 °C. In addition to the filament and substrate temperatures, the ratio of the partial pressure of the monomer to its saturation pressure, is a key parameter in the models for iCVD kinetics and conformal coverage.

From the more than 70 demonstrated monomers used for iCVD to date[75], examples which have been homopolymerized include:

- glycidal methacrylate (GMA, epoxy functionality),
- 2-dimethylamino ethyl methacrylate (DMAEMA, amine functionality),
- 1H,1H,2H,2H-perfluorodecylacryate (PFDA perfluoro functionality),
- hydroxyethylmethacrylate (HEMA, hydroxyl functionality for neutral hydrogels),
- methacrylic acid (MAA, carboxylic acid functionality for pH responsive hydrogels),
- N-isopropylacrylamide (NIPAAm, for thermally responsive hydrogels),
- Zinc (II) meso-tetraphenylporphyrin (ZnTPP) and other porphyrins[73,76].

The vapor phase provides ready mixing of monomers which lack a common solvent, allowing the synthesis of unique copolymers. Indeed amphiphilic surfaces form from iCVD poly(HEMA-co-PFDA)[77] and fuel cell membranes can be fabricated from poly(MAA-co-PFDA)[78].

Crosslinked films result from using at least one iCVD monomer containing two or more unsaturated carbon-carbon bonds. The crosslinking forms in the same step as the iCVD layer growth. No post-treatment is required. In contrast, most solution applied polymers that require post-depositing annealing or UV-exposure to achieve crosslinking.

Crosslinking improves the durability of iCVD polymers and often decreases roughness to sub-nm levels. Demonstrated iCVD crosslinkers include[75]:

- ethylene glycol diacrylate (EGDA),
- ethylene glycol dimethacrylate (EGDMA),
- di(ethylene glycol) divinyl ether (DEGDVE),
- divinyl benzene (DVB),
- allyl methacrylate,
- 2,4,6-trivinyl-2,4,6-trimethyl cyclotrisiloxane (V3D3)
- 2,4,6,8-tetravinyl-2,4,6,8-tetramethyl cyclotetrasiloxane (V4D4)

Pinhole-free films are required for low leakage dielectrics and achieving molecular separation through permselective layers. To avoid pinholes, film roughness must be less than film thickness. Dewetting effects make such ultrathin layers difficult to achieve through solution application. The examples highlighted in Fig. 5a through 5d, each utilized iCVD copolymer layers only 6 to 20 nm thick.

Organic & Hybrid Devices

High performance flexible insulators are essential for next generation flexible and lightweight electronics designed for the Internet of Things (IoT) and wearable device applications.[79] For low power operation, uniform ultrathin (<20 nm) dielectric layers are desired. However, leakage currents tend to increase with decreased film thicknesses.

The ultrasmooth, ultrathin (3-15 nm), flexible, and crosslinked organosilicon layer, poly(2,4,6-trivinyl-2,4,6-trimethyl cyclotrisiloxane) (PV3D3, dielectric constant, k~2.2), has been integrated into devices[80,81], including 3D stacking of organic thin film transistors (TFTs)[82]. The PV3D3 serves as an electret layer when coupled with an ultrathin (20 nm) crosslinked iCVD poly(1,4-butanediol diacrylate) (PBDDA) film as blocking dielectric (Fig. 5a).[83]

Systematic band energy engineering was demonstrated via iCVD copolymerization of V3D3 with 1-vinyl imidazole.[84] In a sub-20 nm thick dielectric formed from HEMA and the crosslinker DEGDVE, segregation of the hydroxyl group of HEMA to the substrate interface produced a hydrophobic skin at the interface with air, reducing leakage current and increasing capacitance.[85] Atomic scale filaments for a memristor comprised of iCVD PV3D3 were integrated into a flexible neural network capable of classifying human faces.[86]

For higher k dielectrics, the iCVD copolymerization of 2-cyanoethyl acrylate and the crosslinker DEGDVE achieved k~6.2.[81] Extension of the iCVD method for ultrathin, flexible, and high-k hybrid organic-inorganic layers for fabricating low-leakage current TFTs.[87,88] The hybrids were obtained by adding of trimethyl alumina or tetrakis-dimethyl-amino-zirconium reactant vapors along HEMA and the TBPO initiator. The metal-containing precursor incorporates into the film

through a condensation reaction between a methyl group on the metal-containing precursor and the hydroxyl functional group of HEMA, in analogy to a commonly utilized reaction for ALD.

Tribodielectric layers for energy harvesting applications have been demonstrated using low-k iCVD fluoropolymers (k~2). Flexible electret films of with high charge stability were fabricated by iCVD polytetrafluoroethylene (PTFE).[89] The performance of triboelectric nanogenerators was systematically investigated for an iCVD fluoropolymer over the thickness range from 0.5 to 12 μm.[90] All-fabric triboelectric generators for wearable electronics were also demonstrated with conformal and breathable iCVD fluoropolymers.[91]

For next-generation electrochemical applications, multiple electronically-insulating nanoscale iCVD organic covalent networks display ionic conduction.[92,93] For lithium ion batteries, a solid electrode interface (SEI) consisting of a conformal, 25 nm thick iCVD organosiloxane, improved the initial coulombic efficiency and capacity retention upon repeated cycling of silicon anodes.[94] The ultrathin and conformal nature of iCVD copolymers from HEMA and a crosslinking monomer are desired for solid-state polymer electrolytes for 3D microbatteries[95] and for stabilizing electroactive polymers[96]

Device Fabrication

For n-type and p-type doping of 3D Fin Field Effect Transistors (FinFETs), iCVD growth of dopant-containing iCVD films utilized the hybrid crosslinking monomers, triallyl phosphate (TAP) and triallyl borate (TAB).[97] The resulting sub-10 nm thick films formed conformally over silicon fins (22 nm width, 100 nm height; 40 nm pitch; Fig. 5b,c). Subsequent rapid thermal annealing (RTA) drives the dopants into the silicon.

Using an ultrathin (~7 nm) iCVD topcoat allowed the directed self-assembly (DSA) of block co-polymers for defining sub-10 nm lines and spaces (Fig. 5d).[98] Conformal, 14-nm thick iCVD wetting layers, enabled successful DSA within the confines of 3D topography.[99] Fine tuning of the surface energy between 39.9 to 42.7 nM/m resulted from changing the filament temperature during iCVD growth from the monomer DVB. Conformal iCVD wetting layers for DSA have subsequently been demonstrated for hole-shrink applications[100] and on complex 3D substrates, including graphene fibers for catalysis applications[101].

Using the high deposition rates possible coupled with near zero intrinsic stress, >10 μm iCVD films grown from the DVB monomer has been exploited to create the spherical shells of targets used for high peak-power lasers (Fig. 5e).[102]

Using a method related to iCVD, provides a new means of altering the 3D nanostructure of a self-assembled block copolymers.[103] Vapors of monomer and initiators infiltrate and swell one of the blocks, which are then photopolymerized. Selective light exposure forms an additional level of hierarchical structure.

For crosslinkers with an asymmetric structure, the reactivity of two unsaturated bonds can differ significantly. For allyl methacrylate, iCVD polymerization proceeded through the acrylic vinyl group.[104] The unreacted pendent allyl functionality can be subsequently crosslinked upon post-

deposition UV exposure, representing a conformal, negative tone resist for solventless patterning.

Rapid flexographic printing requires control of wettability over 3D nanostructured stamps fabricated from arrays of vertically aligned carbon nanotubes (CNTs).[105,106,107] However, the porous stamps collapse when directly wetted by ink and dried. Conformal surface modification of the patterned CNT arrays by an iCVD fluoropolymer before using the stamp eliminates subsequent collapse.

For laminating substrates, parts, and encapsulation layers for flexible and stretchable devices, durability is enhanced by reducing the overall stacking thickness, including the need for thinner adhesive layers. High-shear strength iCVD pressure sensitive adhesives require only 500 nm of thickness[108], a 200-fold reduction over conventional pressure sensitive adhesives. Controlling the degree of crosslinking in the iCVD copolymer led to the viscoelastic behavior required for interfacial bonding.

A different iCVD copolymer, having both epoxy and amine groups, was demonstrated as a dry nanoadhesive.[109] Rapid bonding across the interface results from reaction of these two types of functional groups. No reaction byproducts result and hence, no bubbles form at the interface. Nanoadhesive bonding using the iCVD homopolymer from GMA along with subsequent liquid-application of a diamine, contributed to the fabrication of flexible microfluidic lens arrays.[110] For this iCVD nanoadhesive chemistry, a particularly simple reactor was designed.[111]

Hydrophobic Surfaces

The iCVD homopolymers grown from PFDA, V3D3, V4D4, and DVB form hydrophobic surfaces. Typical surface energies are 8.3, 37.0, 34.9, and 35.1 mN/m, respectively.[112] In addition to low surface energy, surface morphology strongly influences wetting behavior.[113]

The surface roughness of PFDA-containing iCVD fluoropolymers depends on the degree of crystallization, crystallite orientation, nucleation density, and the type, if any, of interfacial grafting was used.[114,115] In situ grafting of a copolymer synthesized from PFDA and DVB results in low rms surface roughness (< 2 nm, Fig. 6a). Ex situ grafting of the same iCVD copolymer using vinyl silane results in an rms surface roughness of 144 nm (Fig. 6b).[116] With these surfaces the more efficient dropwise condensation mechanism could be obtained for low surface tension liquids. The conformal nature of iCVD fluoropolymers allows hydrophobic surface modification of 3D printed parts.[117] Graphene was effectively transferred to paper substrates coated with iCVD hydrophobic homopolymers from PFDA or hexafluorobutylacrylate.[118]

iCVD homopolymerization of V3D3, V4D4, or DVB yields fluorine-free amorphous covalent network displaying low surface roughness(< 2 nm rms).[112] These smooth surface modification layers can outperform the lower surface energy PFDA-containing films for some protective applications, including the reducing the formation of inorganic scale.[112,119] Copolymerization of V4D4 and cyclohexylmethacrylate yielded a smooth, transparent iCVD film with moisture barrier properties of interest for electronics protection.[120]

The PFDA and 1H,1H,2H,2H-perfluorodecyl methacrylate (PFDMA) monomers both possess a C8 [-$(CF_2)_8F$] pendent chain. Additionally, PFDMA has a bulky α-methyl group, leading to films displaying higher glass transition temperatures (T_g).[121] However, the rate of chain propagation leading to polymer film growth is typically ~10x slower for methacrylates, such as PFDMA, than their acrylate counterpart.

Crystallization of side groups is a barrier to surface reconstruction upon wetting. Interestingly, the specific iCVD conditions used determines if the C8 side chains of the PFDA units crystalize perpendicular or parallel to the growth surface.[122] Shorter fluorinated side groups have a reduced propensity to crystalize. Without the need to overcome the enthalpy of crystallization, reorientation of the side groups occurs more easily upon wetting, leading to higher values of contact angle hysteresis (CAH).

Crosslinking tends to restrict side group reorientation on wetting, as is desirable for reducing CAH. The crosslinked films are also typically more durable. Copolymerizing PFDA with the divinyl crosslinker EGDMA improves the resistance to cracking of the resulting iCVD fluoropolymer films.[123] Copolymerizing PFMDA with the tetravinyl organosilicone crosslinker V4D4, lead to films able to withstand >3000 cycles of abrasion testing.[124] Transparent and robust optical protection results from the iCVD copolymerization of PFDA with the epoxy-functional monomer GMA. Annealing these films induces crosslink formation through the ring opening of epoxy groups.[125] The annealed films protect against mechanical abrasion, humidity, liquid water, salt water, and organic solvents. Using a monomer with a C7 side chain[-$(CF_2)_7F$] and known to result in relative high T_g fluoropolymer, 1H,1H-perfluorooctylmethacrylate (H_1F_7MA) copolymerized with DVB provided breathable iCVD water repellent surface modification on a variety of textiles.[121] These films survived 10,000 abrading strokes and ten wash cycles.

Robustness can also be enhanced by engineering the interface with the substrate. The monomer 1H,1H,2H,2H-perfluorooctylacrylate (C6PFA) contains a C6 side chain[-$(CF_2)_6F$] and yields an iCVD homopolymer with high CAH (>90°). Copolymerization with the DVB reduces the CAH, but the lowest CAH (23°) came from a bilayer iCVD strategy in which the first step is growth a crosslinked hydrocarbon base layer from DVB followed by the synthesis an ultrathin top layer from pure C6PFA.[126] Since it is unfavorable for the C6 side chains to reorient into the DVB layer, surface reconstruction upon wetting was limited. The same bilayer strategy proved successful when the fluoromonomer was changed to PFDA. Performing ex situ grafting with vinyl silane, lead to grafted bilayers which survived sand erosion testing.[127]

Nanostructured Surfaces & Composites

Multiple iCVD strategies enable the design of unique nanostructured surfaces. Patterns of micro- and nano- scale features modified conformally by ultrathin iCVD fluoropolymers decrease surface energy while preserving surface texture.[128,113] Alternatively, beginning iCVD fluoropolymer growth on a modestly textured surfaces can result in dramatic morphologies that readily trap air and reduce corrosion rates of the underlying metal (Fig. 6c).[129,130]

By optimizing processing conditions, iCVD can infill porous and textured substrates. The infiltration of iCVD fluoropolymers into TiO_2 nanoparticles matrices produces composite films with high loadings of inorganic particles[131] and bulk hybrid composites acting as superhydrophobic sponges[132]. Modified iCVD processes can achieve global and local planarization of surfaces features on silicon wafers.[133,134]

For all-dry membrane fabrication, monomers were first solidified on a cooled reactor stage in the absence of an initiator.[135,136] The resulting porous microstructures were next infiltrated by an iCVD polymer grown from the same monomer. Sublimation of the solid monomer yields free-standing porous membranes (Fig. 6d).

Combining iCVD polymerization with vapor deposition methods for inorganic materials provides new synthesis options for hybrid materials. Utilizing low vapor pressure ionic liquids as a substrate for iCVD organic particles and metals by dc magnetron sputtering allows fabrication of unique hybrid particles, films, and gels.[137] Alternating the iCVD of organosiloxanes with the ALD of aluminium oxide produces dyads for barrier layer protection of optoelectronic devices.[138]

Smart Surfaces

Variations in humidity, pH, temperature, pH, or light exposure can trigger properties changes in smart materials. Synthesizing responsive polymers by iCVD allows ultrathin layers to grow conformally over micro- and nano-structures for applications in sensing, actuation, membrane separations, and controlled drug delivery.[139]

Utilizing reduced thicknesses accelerates the kinetics of response. Rapid detection of fluctuations of humidity resulted from thin HEMA-based iCVD hydrogels integrated into sensing devices.[140] The observed swelling upon exposed to water vapor followed Flory-Huggins theory. The selection and concentration of crosslinker molecule selected produces systematically varied mesh sizes over the range from 0.15 to 3.1 nm.[96,141,142]

Crosslinked iCVD copolymers of MAA and 4-vinyl pyridine display pH-responsive swelling at pH values of ~3 and ~9, respectively. Growing these materials on opposing sides of a porous substrate creates a Janus membrane.[143] Tuning the iCVD growth conditions to achieve partial conformality, allows keyhole-shaped on-off gates to form over the pore openings. Sequential adjustment of the pH on each side programs the membranes to take in, store, and release proteins on demand (Fig. 7a).

Thermoresponsive iCVD films result from the iCVD copolymerization of a crosslinker with either NIPAAm, N, N-diethylacrylamide, and N-vinylcaprolactam.[144,145,146] These compositions exhibit lower critical solution temperatures (LCST) near body temperature. A swollen hydrophilic state exists below the LCST. Raising the temperature above the LCST induces a rapidly switchable and reversible phase transition to a collapsed hydrophobic state (Fig. 7b,c).

Their mild processing conditions allow iCVD responsive layers to be deposited directly over pharmaceuticals for controlled drug release applications. To control the diffusional release of

drugs, the mesh size of HEMA-based iCVD hydrogels was systematically tuned from ~0.1 to ~0.3 nm, by decreasing the fraction of the EGDMA crosslinking incorporated into the film (Fig. 7d).[142] Conformal coatings of iCVD hydrogels based on HEMA and methacrylic acid over textile substrates layered with drugs hold great promise for improving treatments for wound healing.[147]

Thermally-responsive controlled drug release was also demonstrated for NIPAAm-based iCVD films.[148] Biodegradable and pH responsive iCVD films grown from MAA allow for controlled release of pharmaceuticals through the gradual erosion of the iCVD encapsulating layer.[149]

A nanofiber mat loaded with a chemotherapy agent was conformally coated by a pH sensitive iCVD layer from 4-vinylpyridine and EGDMA.[150] These iCVD coated nanofibers extended the period of reduced the proliferation and stimulated death for U87MG brain cancer cells.

Biotechnology

For interactions with living cells and tissues, surface modification layers must be free of impurities and stable under the conditions of use. A vapor deposition approach eliminates the possibility of contamination by residual solvent. Additionally, purifying iCVD monomers, which are small molecules, is much easier than purifying macromolecular polymer chains. Some crosslinked iCVD networks, such as PV3D3, display remarkable stablity during multiple years of evaluation under physiological conditions.[151] Another advantage is that the conformality of iCVD enables ready encapsulation of medical devices possessing complex geometries.

Surfaces for biomedical application can be designed directly from the library of functional groups processed by iCVD monomers. Post-deposition modification of the iCVD functional groups provides additional options to achieve the precise chemical signaling desired at the surface.

Culturing of human cancer stem cells to form multicellular tumor spheriods was readily, and reproducable achieved on crosslinked iCVD polysiloxane surfaces. [152] The resulting spheroids are desired for drug screening and efficacy testing.

The fast and efficient capture of nucleic acids from cell lysate was demonstrated using a conventional stainless steel mesh filter or an extraction microchip conformally modified with iCVD poly(2-dimethyaminomethyl styrene).[153,154] Under the conditions of extraction, this iCVD surface has a positively charged functional group [$-N^{+}(CH_3)_2$], producing a strong attractions to negatively charged nucleic acids. This method successfully allowed the identification of the DNA from a specific strain of bacteria in multiple types of spoiled food items.

The iCVD method allow uniform coverage of complex 3D surface topologies of devices and membranes for biomedical applications. Polyionic iCVD copolymers based on MAA, DMAEMA, and a crosslinker show promise for surface engineering of neural microelectrodes, reducing adhesion of microglia and surface adsoption of laminin and bovine serum album.[155] The hemocompatability of porous polylactide membranes was significantly enhanced by an iCVD

crosslinked copolymer from MAA and EGDA.[156] Reduce adhesion of microglia and astrocytes was also observed on iCVD hydrogel layers grown from HEMA and holds promise for improving the performance of shunts for draining excess cerebrospinal fluid of hydrocephalus patients.[157]

A robust crosslinked ionic iCVD copolymer surface displayed the promotion of mammalian cell growth while simultaneously killing bacterial cells.[158] Reacting vapors of 4-vinylbenzyl chloride and DMAEMA produced quaternary ammonium sites ($-N^+R_3\,Cl^-$). These ionic sites are responsible for both the observed antimicrobial activity and crosslinking of the organic iCVD network. The antimicrobial coating was sucessfully applied to multiple types of plastic as well as to titanium.

The epoxy functional group of the monomer GMA undergoes facile ring opening reactions with amine functional groups. Thus, GMA-containing iCVD surfaces can readily be conjucated with bioactive molecules, including peptides and amine-containing polymers. For improving the biocompatiblity of the titanium implants commonly used in bone repair and joint replacement, the GMA units were successfully functionalized with a protein that promote rapid healing of damage boned tissue.[159] The epoxy moieties of GMA were also successfully employed to immobilize polyethyleneimine, as a blanket or patterned layer, to provide an adhesion site for lentivirus.[160] Patterned viral functionalized surfaces allowed for site-specific delivery of viral genes to cultured human tissue.

Conclusions

Control over nanostructure and defect levels provides a means to understand, design, and optimize the properties of polymer layers by oCVD and iCVD. Both are all-dry processes employing modest growth temperatures and which scale-up to large reactors. The resulting organic and hybrid layers can conform to complex surface geometries.

Using the oCVD step growth of conjugated polymers provides controlled nanotexture. The optimized characteristics are attractive for flexible transparent conducting electrodes for multiple applications, including photovoltaics and wearable devices. Improved electrochemical energy storage has be demonstrated with ultrathin and conformal oCVD polymers in both batteries and supercapacitor devices. Additionally, promising electrocatalysis results have been achieved using oCVD.

The iCVD method has synthesized a wide variety of chain-growth homopolymers and copolymers. Multiple iCVD compositions have been integrated directly into next-generation devices, including those desired for wearable electronics and the IoT. Examples include dielectrics for flexible TFTs, 3D microbatteries, and triboelectric energy harvesting, having order of magnitude thicknesses of 10 nm, 100 nm, and 1000 nm, respectively. Additionally, advanced doping and lithography processes for sub-10 nm semiconductor device fabrication have been demonstrated using iCVD layers. Some iCVD compositions provide a protective barrier against humidity, wetting, corrosion, inorganic scaling, and biofouling. Other iCVD layers create selective permeation layers of interest for molecular separations, sensing, and controlled drug

release. The high density of reactive functional groups possible on iCVD surfaces enables nanoadhesion and post-deposition functionalization with biomolecules. Additionally, these functional groups can produce property changes in response to temperature, pH, or light, and form the basis for iCVD "smart" surfaces.

These applications, and many others, are expected to benefit from the continued development of processes for CVD polymers. The theories developed for organic polymers and inorganic thin films have both significantly aided the fundamental understanding of CVD polymer thin films and processes.

References

1. *CVD Polymers: Fabrication of Organic Surfaces and Devices*. (Wiley, 2015).
2. Wang, M., Wang, X., Moni, P., Liu, A., Kim, D. H., Jo, W. J., Sojoudi, H. & Gleason, K. K. CVD Polymers for Devices and Device Fabrication. *Adv. Mater.* **29**, 1604606 (2017).
3. Odian, G. *Principles of Polymerization*. *Principles of Polymerization* (John Wiley & Sons, Inc., 2004). doi:10.1002/047147875X
4. Lock, J. P., Im, S. G. & Gleason, K. K. Oxidative Chemical Vapor Deposition of Electrically Conducting Poly(3,4-ethylenedioxythiophene) Films. *Macromolecules* **39**, 5326–5329 (2006).
5. Heydari Gharahcheshmeh, M. & Gleason, K. K. Device Fabrication Based on Oxidative Chemical Vapor Deposition (oCVD) Synthesis of Conducting Polymers and Related Conjugated Organic Materials. *Adv. Mater. Interfaces* **6**, 1801564 (2019).
6. Mao, Y. & Gleason, K. K. Hot filament chemical vapor deposition of poly(glycidyl methacrylate) thin films using tert-butyl peroxide as an initiator. *Langmuir* **20**, 2484–2488 (2004).
7. Matsumura, H., Umemoto, H., Gleason, K. K. & Schropp, R. E. I. *Catalytic Chemical Vapor Deposition*. *Catalytic Chemical Vapor Deposition Technology* (Wiley, 2019). doi:10.1002/9783527818655
8. Gleason, K. K. Chemically Vapor Deposited Polymer Nanolayers for Rapid and Controlled Permeation of Molecules and Ions. *J. Vac. Sci. Technol. A* **38**, (2020).
9. George, S. M., Dameron, A. A. & Yoon, B. Surface chemistry for molecular layer deposition of organic and hybrid organic-inorganic polymers. *Acc. Chem. Res.* **42**, 498–508 (2009).
10. Zhou, H. & Bent, S. F. Fabrication of organic interfacial layers by molecular layer deposition: Present status and future opportunities. *J. Vac. Sci. Technol. A* **31**, 040801 (2013).
11. Chen, H. Y. & Lahann, J. Designable biointerfaces using vapor-based reactive polymers. *Langmuir* **27**, 34–48 (2011).
12. Hassan, Z., Spuling, E., Knoll, D. M. & Bräse, S. Regioselective Functionalization of

[2.2]Paracyclophanes: Recent Synthetic Progress and Perspectives. *Angew. Chemie - Int. Ed.* **58**, 2–17 (2019).

13. Gupta, M. & Gleason, K. K. Large-scale initiated chemical vapor deposition of poly(glycidyl methacrylate) thin films. *Thin Solid Films* **515**, 1579–1584 (2006).

14. Kovacik, P., Del Hierro, G., Livernois, W. & Gleason, K. K. Scale-up of oCVD: Large-area conductive polymer thin films for next-generation electronics. *Mater. Horizons* **2**, 221–227 (2015).

15. Yilmaz, K., Sakalak, H., Gürsoy, M. & Karaman, M. Initiated Chemical Vapor Deposition of Poly(Ethylhexyl Acrylate) Films in a Large-Scale Batch Reactor. *Ind. Eng. Chem. Res.* **58**, 14795–14801 (2019).

16. Cheng, C. & Gupta, M. Roll-to-Roll Surface Modification of Cellulose Paper via Initiated Chemical Vapor Deposition. *Ind. Eng. Chem. Res.* **57**, 11675–11680 (2018).

17. Pryce Lewis, H. G., Bansal, N. P., White, A. J. & Handy, E. S. HWCVD of polymers: Commercialization and scale-up. *Thin Solid Films* **517**, 3551–3554 (2009).

18. Bilger, D., Homayounfar, S. Z. & Andrew, T. L. A critical review of reactive vapor deposition for conjugated polymer synthesis. *J. Mater. Chem. C* **7**, 7159–7174 (2019).

19. Baba, K., Bengasi, G., El Assad, D., Grysan, P., Lentzen, E., Heinze, K., Frache, G. & Boscher, N. D. Conductive Directly Fused Poly(Porphyrin) Coatings by Oxidative Chemical Vapour Deposition – From Single- to Triple-Fused. *European J. Org. Chem.* **2019**, 2368–2375 (2019).

20. Schöfberger, W., Zheng, X., Stifter, D., Kus, M., Liu, M., Greunz, T., Coskun, H., Farka, D., Sariciftci, N. S., Stadler, P., *et al.* Biofunctionalized conductive polymers enable efficient CO 2 electroreduction. *Sci. Adv.* **3**, e1700686 (2017).

21. Im, S. G., Kusters, D., Choi, W., Baxamusa, S. H., Sanden, M. C. M. Van De & Gleason, K. K. Conformal Coverage of Poly(3,4- ethylenedioxythiophene) Films with Tunable Nanoporosity. **2**, 1959–1967 (2008).

22. Atanasov, S. E., Losego, M. D., Gong, B., Sachet, E., Maria, J. P., Williams, P. S. & Parsons, G. N. Highly conductive and conformal poly(3,4-ethylenedioxythiophene) (PEDOT) thin films via oxidative molecular layer deposition. *Chem. Mater.* **26**, 3471–3478 (2014).

23. Nejati, S. & Lau, K. K. S. Chemical vapor deposition synthesis of tunable unsubstituted polythiophene. *Langmuir* **27**, 15223–15229 (2011).

24. Smolin, Y. Y., Soroush, M. & Lau, K. K. S. Influence of oCVD Polyaniline Film Chemistry in Carbon-Based Supercapacitors. *Ind. Eng. Chem. Res.* **56**, 6221–6228 (2017).

25. Farka, D., Coskun, H., Gasiorowski, J., Cobet, C., Hingerl, K., Uiberlacker, L. M., Hild, S., Greunz, T., Stifter, D., Sariciftci, N. S., *et al.* Anderson-Localization and the Mott–Ioffe–Regel Limit in Glassy-Metallic PEDOT. *Adv. Electron. Mater.* **3**, 1700050 (2017).

26. Chelawat, H., Vaddiraju, S. & Gleason, K. Conformal, Conducting Poly(3,4-

ethylenedioxythiophene) Thin Films Deposited Using Bromine as the Oxidant in a Completely Dry Oxidative Chemical Vapor Deposition Process. *Chem. Mater.* **22**, 2864–2868 (2010).

27. Im, S. G. G., Yoo, P. J. J., Hammond, P. T. T. & Gleason, K. K. K. Grafted Conducting Polymer Films for Nano-patterning onto Various Organic and Inorganic Substrates by Oxidative Chemical Vapor Deposition. *Adv. Mater.* **19**, 2863–2867 (2007).

28. Trujillo, N. J., Barr, M. C., Im, S. G. & Gleason, K. K. Oxidative chemical vapor deposition (oCVD) of patterned and functional grafted conducting polymer nanostructures. *J. Mater. Chem.* **20**, 3968–3972 (2010).

29. Ugur, A., Katmis, F., Li, M., Wu, L., Zhu, Y., Varanasi, K. K. & Gleason, K. K. Low-Dimensional Conduction Mechanisms in Highly Conductive and Transparent Conjugated Polymers. *Adv. Mater.* **27**, 4604–4610 (2015).

30. Lassnig, A., Nakamura, N., Jörg, T., Reeja-Jayan, B. & Cordill, M. J. Molecularly grafted, structurally integrated multifunctional polymer thin films with improved adhesion. *Surf. Coatings Technol.* **349**, 963–968 (2018).

31. Ibanez, J. G., Rincón, M. E., Gutierrez-Granados, S., Chahma, M., Jaramillo-Quintero, O. A. & Frontana-Uribe, B. A. Conducting Polymers in the Fields of Energy, Environmental Remediation, and Chemical-Chiral Sensors. *Chem. Rev.* **118**, 4731–4816 (2018).

32. Petsagkourakis, I., Kim, N., Tybrandt, K., Zozoulenko, I. & Crispin, X. Poly(3,4-ethylenedioxythiophene): Chemical Synthesis, Transport Properties, and Thermoelectric Devices. *Adv. Electron. Mater.* **5**, 1800918 (2019).

33. Gharahcheshmeh, M. H., Tavakoli, M. M. & Gleason, E. F. Tuning , optimization , and perovskite solar cell device integration of ultrathin poly (3 , 4-ethylene dioxythiophene) films via a single-step all-dry process. *Sci. Adv.* **5**, eaay0414 (2019).

34. Jaros, A., Bley, S., Zimmermann, K., Krieg, L., Castro-Carranza, A., Gutowski, J., Meierhofer, F. & Voss, T. Optical Properties and Carrier Dynamics in Inorganic and Hybrid Inorganic/Organic ZnO- and GaN-Based Nanowire Structures. *Phys. Status Solidi Basic Res.* **256**, 1800463 (2019).

35. Barr, M. C., Rowehl, J. a, Lunt, R. R., Xu, J., Wang, A., Boyce, C. M., Im, S. G., Bulović, V. & Gleason, K. K. Direct monolithic integration of organic photovoltaic circuits on unmodified paper. *Adv. Mater.* **23**, 3499–3505 (2011).

36. Andrew, T. L., Zhang, L., Cheng, N., Baima, M., Kim, J. J., Allison, L. & Hoxie, S. Melding Vapor-Phase Organic Chemistry and Textile Manufacturing to Produce Wearable Electronics. *Acc. Chem. Res.* **51**, 850–859 (2018).

37. Wang, X., Zhang, X., Sun, L., Lee, D., Lee, S., Wang, M., Zhao, J., Shao-Horn, Y., Dincă, M., Palacios, T., *et al.* High electrical conductivity and carrier mobility in oCVD PEDOT thin films by engineered crystallization and acid treatment. *Sci. Adv.* **4**, eaat5780 (2018).

38. Gueye, M. N., Carella, A., Faure-Vincent, J., Demadrille, R. & Simonato, J.-P. Progress in understanding structure and transport properties of PEDOT-based materials: A critical review. *Prog. Mater. Sci.* **108**, 100616 (2019).

39. Minami, T. Transparent conducting oxide semiconductors for transparent electrodes. *Semicond. Sci. Technol.* **20**, S37 (2005).

40. Abessolo Ondo, D., Loyer, F., Chemin, J. B., Bulou, S., Choquet, P. & Boscher, N. D. Atmospheric plasma oxidative polymerization of ethylene dioxythiophene (EDOT) for the large-scale preparation of highly transparent conducting thin films. *Plasma Process. Polym.* **15**, e1700172 (2018).

41. Farka, D., Jones, A. O. F., Menon, R., Sariciftci, N. S. & Stadler, P. Metallic conductivity beyond the Mott minimum in PEDOT: Sulphate at low temperatures. *Synth. Met.* **240**, 59–66 (2018).

42. Xu, Y., Wang, X., Zhou, J., Song, B., Huberman, S., Chen, G., Wang, X., Lee, E. M. Y., Gleason, K. K. & Jiang, Z. Molecular engineered conjugated polymer with high thermal conductivity. *Sci. Adv.* **4**, eaar3031 (2018).

43. Moni, P., Lau, J., Mohr, A. C., Lin, T. C., Tolbert, S. H., Dunn, B. & Gleason, K. K. Growth Temperature and Electrochemical Performance in Vapor-Deposited Poly(3,4-ethylenedioxythiophene) Thin Films for High-Rate Electrochemical Energy Storage. *ACS Appl. Energy Mater.* **1**, 7093–7105 (2018).

44. Klemens, P. G. Phonon scattering and thermal resistance due to grain boundaries. *Int. J. Thermophys.* **15**, 1345–1351 (1994).

45. Franco-Gonzalez, J. F. & Zozoulenko, I. V. Molecular Dynamics Study of Morphology of Doped PEDOT: From Solution to Dry Phase. *J. Phys. Chem. B* **121**, 4299–4307 (2017).

46. Noriega, R., Rivnay, J., Vandewal, K., Koch, F. P. V., Stingelin, N., Smith, P., Toney, M. F. & Salleo, A. A general relationship between disorder, aggregation and charge transport in conjugated polymers. *Nat. Mater.* **12**, 1038–1044 (2013).

47. Mollinger, S. A., Krajina, B. A., Noriega, R., Salleo, A. & Spakowitz, A. J. Percolation, Tie-Molecules, and the Microstructural Determinants of Charge Transport in Semicrystalline Conjugated Polymers. *ACS Macro Lett.* **4**, 708–712 (2015).

48. Drewelow, G., Wook Song, H., Jiang, Z. T. & Lee, S. Factors controlling conductivity of PEDOT deposited using oxidative chemical vapor deposition. *Appl. Surf. Sci.* **501**, 144105 (2020).

49. Lee, S., Paine, D. C. & Gleason, K. K. Heavily doped poly(3,4-ethylenedioxythiophene) thin films with high carrier mobility deposited using oxidative CVD: Conductivity stability and carrier transport. *Adv. Funct. Mater.* **24**, 7187–7196 (2014).

50. Salaneck, W. R., Friend, R. H. & Brédas, J. L. Electronic structure of conjugated polymers: consequences of electron–lattice coupling. *Phys. Rep.* **319**, 231–251 (1999).

51. Heeger, A. J., Sarichiftci, N. S. & Namdas, E. B. *Semiconducting and Metallic Polymers*. (Oxford Univ. Press, 2010).

52. Rolland, N., Franco-Gonzalez, J. F. & Zozoulenko, I. Can Mobility Negative Temperature Coefficient Be Reconciled with the Hopping Character of Transport in Conducting Polymers? *ACS Appl. Polym. Mater.* **1**, 2833–2839 (2019).

53. Lee, S., Borrelli, D. C., Jo, W. J., Reed, A. S. & Gleason, K. K. Nanostructured Unsubstituted Polythiophene Films Deposited Using Oxidative Chemical Vapor Deposition: Hopping Conduction and Thermal Stability. *Adv. Mater. Interfaces* **5**, 1701513 (2018).

54. Arnold, S. P., Harris, J. K., Neelamraju, B., Rudolph, M. & Ratcliff, E. L. Microstructure-dependent electrochemical properties of chemical-vapor deposited poly(3,4-ethylenedioxythiophene) (PEDOT) films. *Synth. Met.* **253**, 26–33 (2019).

55. Zhang, L. & Andrew, T. L. Deposition Dependent Ion Transport in Doped Conjugated Polymer Films: Insights for Creating High-Performance Electrochemical Devices. *Adv. Mater. Interfaces* **4**, 1700873 (2017).

56. Evans, D., Fabretto, M., Mueller, M., Zuber, K., Short, R. & Murphy, P. Structure-directed growth of high conductivity PEDOT from liquid-like oxidant layers during vacuum vapor phase polymerization. *J. Mater. Chem.* **22**, 14889–14895 (2012).

57. Xu, G. L., Liu, Q., Lau, K. K. S., Liu, Y., Liu, X., Gao, H., Zhou, X., Zhuang, M., Ren, Y., Li, J., *et al.* Building ultraconformal protective layers on both secondary and primary particles of layered lithium transition metal oxide cathodes. *Nat. Energy* **4**, 484–494 (2019).

58. Su, L., Smith, P. M., Anand, P. & Reeja-Jayan, B. Surface Engineering of a LiMn 2 O 4 Electrode Using Nanoscale Polymer Thin Films via Chemical Vapor Deposition Polymerization. *ACS Appl. Mater. Interfaces* **10**, 27063–27073 (2018).

59. Nejati, S., Minford, T. E., Smolin, Y. Y. & Lau, K. K. S. Enhanced charge storage of ultrathin polythiophene films within porous nanostructures. *ACS Nano* **8**, 5413–5422 (2014).

60. Zhou, Y., Wang, X., Acauan, L., Kalfon-Cohen, E., Ni, X., Stein, Y., Gleason, K. K. & Wardle, B. L. Ultrahigh-Areal-Capacitance Flexible Supercapacitor Electrodes Enabled by Conformal P3MT on Horizontally Aligned Carbon-Nanotube Arrays. *Adv. Mater.* **31**, 1901916 (2019).

61. Lachman, N., Stein, I. Y., Ugur, A., Lidston, D. L., Gleason, K. K. & Wardle, B. L. Synthesis of polymer bead nano-necklaces on aligned carbon nanotube scaffolds. *Nanotechnology* **28**, 24LT01 (2017).

62. Lachman, N., Xu, H., Zhou, Y., Ghaffari, M., Lin, M., Bhattacharyya, D., Ugur, A., Gleason, K. K., Zhang, Q. M. & Wardle, B. L. Tailoring thickness of conformal conducting polymer decorated aligned carbon nanotube electrodes for energy storage. *Adv. Mater. Interfaces* **1**, 1400076 (2014).

63. Smolin, Y. Y., Van Aken, K. L., Boota, M., Soroush, M., Gogotsi, Y. & Lau, K. K. S. Engineering Ultrathin Polyaniline in Micro/Mesoporous Carbon Supercapacitor Electrodes Using Oxidative Chemical Vapor Deposition. *Adv. Mater. Interfaces* **4**, 1601201 (2017).

64. Liu, A., Kovacik, P., Peard, N., Tian, W., Goktas, H., Lau, J., Dunn, B. & Gleason, K. K. Monolithic Flexible Supercapacitors Integrated into Single Sheets of Paper and Membrane

via Vapor Printing. *Adv. Mater.* **29**, 160691 (2017).

65. Zhang, L. & Andrew, T. L. Using the Surface Features of Plant Matter to Create All-Polymer Pseudocapacitors with High Areal Capacitance. *ACS Appl. Mater. Interfaces* **10**, 38574–38580 (2018).

66. Kim, J. J., Allison, L. K. & Andrew, T. L. Vapor-printed polymer electrodes for long-term, on-demand health monitoring. *Sci. Adv.* **5**, eaaw0463 (2019).

67. Kaviani, S., Mohammadi Ghaleni, M., Tavakoli, E. & Nejati, S. Electroactive and Conformal Coatings of Oxidative Chemical Vapor Deposition Polymers for Oxygen Electroreduction. *ACS Appl. Polym. Mater.* **1**, 552–560 (2019).

68. Smith, P. M., Su, L., Gong, W., Nakamura, N., Reeja-Jayan, B. & Shen, S. Thermal conductivity of poly(3,4-ethylenedioxythiophene) films engineered by oxidative chemical vapor deposition (oCVD). *RSC Adv.* **8**, 19348–19352 (2018).

69. Bose, R. K., Nejati, S., Stufflet, D. R. & Lau, K. K. S. Graft polymerization of anti-fouling PEO surfaces by liquid-free initiated chemical vapor deposition. *Macromolecules* **45**, 6915–6922 (2012).

70. Gao, Y., Cole, B. & Tenhaeff, W. E. Chemical Vapor Deposition of Polymer Thin Films Using Cationic Initiation. *Macromol. Mater. Eng.* **303**, 1700425 (2018).

71. Chan, K. & Gleason, K. K. Photoinitiated chemical vapor deposition of polymeric thin films using a volatile photoinitiator. *Langmuir* **21**, 11773–11779 (2005).

72. Martin, T. P., Sedransk, K. L., Chan, K., Baxamusa, S. H. & Gleason, K. K. Solventless Surface Photoinitiated Polymerization: Grafting Chemical Vapor Deposition (gCVD). *Macromolecules* **40**, 4586–4591 (2007).

73. Boscher, N. D., Wang, M., Perrotta, A., Heinze, K., Creatore, M. & Gleason, K. K. Metal–Organic Covalent Network Chemical Vapor Deposition for Gas Separation. *Adv. Mater.* **28**, 7479–7485 (2016).

74. Loyer, F., Bulou, S., Choquet, P. & Boscher, N. D. Pulsed plasma initiated chemical vapor deposition (PiCVD) of polymer layers − A kinetic model for the description of gas phase to surface interactions in pulsed plasma discharges. *Plasma Process. Polym.* **15**, (2018).

75. Gleason, K. K. Organic Surface Modification by Initiated CVD (iCVD). in *Surface Modification of Polymers: Methods and Applications* (eds. Pinson, J. & Thiry, D.) (Wiley, 2019).

76. Wang, M., Boscher, N. D., Heinze, K. & Gleason, K. K. Gas Selective Ultrathin Organic Covalent Networks Synthesized by iPECVD: Does the Central Metal Ion Matter? *Adv. Funct. Mater.* **27**, 1606652 (2017).

77. Baxamusa, S. H. & Gleason, K. K. Random copolymer films with molecular-scale compositional heterogeneities that interfere with protein adsorption. *Adv. Funct. Mater.* **19**, 3489–3496 (2009).

78. Coclite, A. M., Lund, P., Di Mundo, R. & Palumbo, F. Novel hybrid fluoro-carboxylated

copolymers deposited by initiated chemical vapor deposition as protonic membranes. *Polymer (Guildf).* **54**, 24–30 (2013).

79. Wang, Y., Huang, X., Li, T., Li, L., Guo, X. & Jiang, P. Polymer-Based Gate Dielectrics for Organic Field-Effect Transistors. *Chem. Mater.* **31**, 2212–2240 (2019).

80. Moon, H., Seong, H., Shin, W. C., Park, W. T., Kim, M., Lee, S., Bong, J. H., Noh, Y. Y., Cho, B. J., Yoo, S., *et al.* Synthesis of ultrathin polymer insulating layers by initiated chemical vapour deposition for low-power soft electronics. *Nat. Mater.* **14**, 628–635 (2015).

81. Yang, S. C., Choi, J., Jang, B. C., Hong, W., Shim, G. W., Yang, S. Y., Im, S. G. & Choi, S. Y. Large-Scale, Low-Power Nonvolatile Memory Based on Few-Layer MoS 2 and Ultrathin Polymer Dielectrics. *Adv. Electron. Mater.* **5**, 1800688 (2019).

82. Yoo, H., Park, H., Yoo, S., On, S., Seong, H., Im, S. G. & Kim, J. J. Highly stacked 3D organic integrated circuits with via-hole-less multilevel metal interconnects. *Nat. Commun.* **10**, 10:2424 (2019).

83. Pak, K., Choi, J., Lee, C. & Im, S. G. Low-Power, Flexible Nonvolatile Organic Transistor Memory Based on an Ultrathin Bilayer Dielectric Stack. *Adv. Electron. Mater.* **5**, 1800799 (2019).

84. Oh, J. G., Pak, K., Kim, C. S., Bong, J. H., Hwang, W. S., Im, S. G. & Cho, B. J. A High-Performance Top-Gated Graphene Field-Effect Transistor with Excellent Flexibility Enabled by an iCVD Copolymer Gate Dielectric. *Small* **14**, 1703035 (2018).

85. Choi, J., Yoon, J., Kim, M. J., Pak, K., Lee, C., Lee, H., Jeong, K., Ihm, K., Yoo, S., Cho, B. J., *et al.* Spontaneous Generation of a Molecular Thin Hydrophobic Skin Layer on a Sub-20 nm, High- k Polymer Dielectric for Extremely Stable Organic Thin-Film Transistor Operation . *ACS Appl. Mater. Interfaces* **11**, 29113–29123 (2019).

86. Jang, B. C., Kim, S., Yang, S. Y., Park, J., Cha, J. H., Oh, J., Choi, J., Im, S. G., Dravid, V. P. & Choi, S. Y. Polymer Analog Memristive Synapse with Atomic-Scale Conductive Filament for Flexible Neuromorphic Computing System. *Nano Lett.* **19**, 839–849 (2019).

87. Kim, M. J., Pak, K., Hwang, W. S., Im, S. G. & Cho, B. J. Novel Vapor-Phase Synthesis of Flexible, Homogeneous Organic-Inorganic Hybrid Gate Dielectric with sub 5 nm Equivalent Oxide Thickness. *ACS Appl. Mater. Interfaces* **10**, 37326–37334 (2018).

88. Kim, M. J., Pak, K., Choi, J., Lee, T. I., Hwang, W. S., Im, S. G. & Cho, B. J. Ultrathin ZrO x -Organic Hybrid Dielectric (EOT 3.2 nm) via Initiated Chemical Vapor Deposition for High-Performance Flexible Electronics. *ACS Appl. Mater. Interfaces* **11**, 44513–4452 (2019).

89. Schröder, S., Strunskus, T., Rehders, S., Gleason, K. K. & Faupel, F. Tunable polytetrafluoroethylene electret films with extraordinary charge stability synthesized by initiated chemical vapor deposition for organic electronics applications. *Sci. Rep.* **9**, 9:2237 (2019).

90. Kim, D., Kim, W. G., Jin, I. K., Park, H., Im, S. G. & Choi, Y. K. A study of the charge distribution and output characteristics of an ultra-thin tribo-dielectric layer. *Nano Energy*

62, 458–464 (2019).

91. Wanwong, S., Sangkhun, W., Homayounfar, S. Z., Park, K. W. & Andrew, T. L. Wash-stable, oxidation resistant conductive cotton electrodes for wearable electronics. *RSC Adv.* **9**, 9198–9203 (2019).

92. Chen, N., Reeja-Jayan, B., Liu, A., Lau, J., Dunn, B. & Gleason, K. K. iCVD Cyclic Polysiloxane and Polysilazane as Nanoscale Thin-Film Electrolyte: Synthesis and Properties. *Macromol. Rapid Commun.* **37**, 446–452 (2016).

93. Sassin, M. B., Long, J. W., Wallace, J. M. & Rolison, D. R. Routes to 3D conformal solid-state dielectric polymers: electrodeposition versus initiated chemical vapor deposition. *Mater. Horizons* **2**, 502–508 (2015).

94. Shen, B. H., Wang, S. & Tenhaeff, W. E. Ultrathin conformal polycyclosiloxane films to improve silicon cycling stability. *Sci. Adv.* **5**, eaaw4856 (2019).

95. Li, W., Bradley, L. C. & Watkins, J. J. Copolymer Solid-State Electrolytes for 3D Microbatteries via Initiated Chemical Vapor Deposition. *ACS Appl. Mater. Interfaces* **11**, 5668–5674 (2019).

96. Mao, X., Liu, A., Tian, W., Wang, X., Gleason, K. K. & Hatton, T. A. Enhancing Performance Stability of Electrochemically Active Polymers by Vapor-Deposited Organic Networks. *Adv. Funct. Mater.* **28**, 1706028 (2018).

97. Kim, J. H., Park, H. K., Pak, K. Y., Yoon, A., Kim, Y. S., Im, S. G., Hwang, W. S. & Cho, B. J. Conformal, Wafer-Scale and Controlled Nanoscale Doping of Semiconductors Via the iCVD Process. in *2018 IEEE International Electron Devices Meeting (IEDM)* **2018-Decem**, 11.1.1-11.1.4 (IEEE, 2018).

98. Suh, H. S., Kim, D. H., Moni, P., Xiong, S., Ocola, L. E., Zaluzec, N. J., Gleason, K. K. & Nealey, P. F. Sub-10-nm patterning via directed self-assembly of block copolymer films with a vapour-phase deposited topcoat. *Nat. Nanotechnol.* **12**, 575–581 (2017).

99. Moni, P., Suh, H. S., Dolejsi, M., Kim, D. H., Mohr, A. C., Nealey, P. F. & Gleason, K. K. Ultrathin and Conformal Initiated Chemical-Vapor-Deposited Layers of Systematically Varied Surface Energy for Controlling the Directed Self-Assembly of Block CoPolymers. *Langmuir* **34**, 4494–4502 (2018).

100. Dolejsi, M., Moni, P., Bezik, C. T., Zhou, C., de Pablo, J. J., Gleason, K. K. & Nealey, P. F. Ultrathin initiated chemical vapor deposition polymer interfacial energy control for directed self-assembly hole-shrink applications. *J. Vac. Sci. Technol. B* **37**, 061804 (2019).

101. Yang, G. G., Choi, J., Cha, S. K., Lee, G. Y., Jin, H. M., Hwang, H. S., Yun, T., Kang, J., Han, K. H., Kim, J. H., *et al.* Conformal 3D Nanopatterning by Block Copolymer Lithography with Vapor-Phase Deposited Neutral Adlayer. *ACS Nano* **13**, 13092–13099 (2019).

102. Baxamusa, S. H., Lepro, X., Lee, T., Worthington, M., Ehrmann, P., Laurence, T., Teslich, N., Suresh, A. & Burkey, D. D. Initiated chemical vapor deposition polymers for high peak-power laser targets. *Thin Solid Films* 37–41 (2017).

103. Qiang, Z., Akolawala, S. A. & Wang, M. Simultaneous In-Film Polymer Synthesis and Self-Assembly for Hierarchical Nanopatterns. *ACS Macro Lett.* **7**, 566–571 (2018).

104. Yang, H., Wang, H., Feng, J., Ye, Y. & Liu, W. Solventless Synthesis and Patterning of UV-Responsive Poly(allyl methacrylate) Film. *Macromol. Chem. Phys.* **220**, 190029 (2019).

105. Kim, S., Sojoudi, H., Zhao, H., Mariappan, D., McKinley, G. H., Gleason, K. K. & Hart, A. J. Ultrathin high-resolution flexographic printing using nanoporous stamps. *Sci. Adv.* **2**, e1601660 (2016).

106. Mariappan, D., Kim, S., Boutilier, M. S. H., Zhao, J., Zhao, H., Beroz, J., Muecke, U., Sojoudi, H., Gleason, K. K., Brun, P.-T., *et al.* Dynamics of Liquid Transfer from Nanoporous Stamps in High-Resolution Flexographic Printing. *Langmuir* **35**, 7659–7671 (2019).

107. Sojoudi, H., Kim, S., Zhao, H., Annavarapu, R. K., Mariappan, D., Hart, A. J., McKinley, G. H. & Gleason, K. K. Stable Wettability Control of Nanoporous Microstructures by iCVD Coating of Carbon Nanotubes. *ACS Appl. Mater. Interfaces* **9**, 43287–43299 (2017).

108. Moon, H., Jeong, K., Kwak, M. J., Choi, S. Q. & Im, S. G. Solvent-Free Deposition of Ultrathin Copolymer Films with Tunable Viscoelasticity for Application to Pressure-Sensitive Adhesives. *ACS Appl. Mater. Interfaces* **10**, 32668–32677 (2018).

109. Kwak, M. J., Kim, D. H., You, J. B., Moon, H., Joo, M., Lee, E. & Im, S. G. A Sub-minute Curable Nanoadhesive with High Transparency, Strong Adhesion, and Excellent Flexibility. *Macromolecules* **51**, 992–1001 (2018).

110. Seo, S., Kim, J., Choi, Y. han, You, J. B., Im, S. G. & Lee, W. Parylene based thin-film microfluidic lens array fabricated by iCVD nano-adhesive bonding. *Polymer (Guildf).* **181**, 121763 (2019).

111. Randall, G. C., Gonzalez, L., Petzoldt, R. & Elsner, F. An Evaporative Initiated Chemical Vapor Deposition Coater for Nanoglue Bonding. *Adv. Eng. Mater.* **20**, 1700839 (2018).

112. Sojoudi, H., Nemani, S. K., Mullin, K. M., Wilson, M. G., Aladwani, H., Lababidi, H. & Gleason, K. K. Micro-/Nanoscale Approach for Studying Scale Formation and Developing Scale-Resistant Surfaces. *ACS Appl. Mater. Interfaces* **11**, 7330–7337 (2019).

113. Annavarapu, R. K., Kim, S., Wang, M., Hart, A. J. & Sojoudi, H. Explaining Evaporation-Triggered Wetting Transition Using Local Force Balance Model and Contact Line-Fraction. *Sci. Rep.* **9**, 9:405 (2019).

114. Coclite, A. M., Shi, Y. & Gleason, K. K. Controlling the degree of crystallinity and preferred crystallographic orientation in poly-perfluorodecylacrylate thin films by initiated chemical vapor deposition. *Adv. Funct. Mater.* **22**, 2167–2176 (2012).

115. Coclite, A. M., Shi, Y. & Gleason, K. K. Grafted crystalline poly-perfluoroacrylate structures for superhydrophobic and oleophobic functional coatings. *Adv. Mater.* **24**, 4534–4539 (2012).

116. Khalil, K., Soto, D., Farnham, T., Paxson, A., Katmis, A. U., Gleason, K. & Varanasi, K. K. Grafted Nanofilms Promote Dropwise Condensation of Low-Surface-Tension Fluids for High-Performance Heat Exchangers. *Joule* **3**, 1377–1388 (2019).

117. Cheng, C. & Gupta, M. Surface functionalization of 3D-printed plastics via initiated chemical vapor deposition. *Beilstein J. Nanotechnol.* **8**, 1629–1639 (2017).

118. Çıtak, E., İstanbullu, B., Şakalak, H., Gürsoy, M. & Karaman, M. All-Dry Hydrophobic Functionalization of Paper Surfaces for Efficient Transfer of CVD Graphene. *Macromol. Chem. Phys.* **220**, 1900277 (2019).

119. Zhao, J., Wang, M., Jebutu, M. S., Zhu, M. & Gleason, K. Fundamental Nanoscale Surface Strategies for Robustly Controlling Heterogeneous Nucleation of Calcium Carbonate. *J. Mater. Chem. A* **7**, 17242–17247 (2019).

120. Seok, J. H., Kim, S. H., Cho, S. M., Yi, G. R. & Lee, J. Y. Crosslinked Organosilicon-Acrylate Copolymer Moisture Barrier Thin Film Fabricated by Initiated Chemical Vapor Deposition (iCVD). *Macromol. Res.* **26**, 1257–1264 (2018).

121. Soto, D., Ugur, A., Farnham, T. A., Gleason, K. K. & Varanasi, K. K. Short-Fluorinated iCVD Coatings for Nonwetting Fabrics. *Adv. Funct. Mater.* **28**, 1707355 (2018).

122. Perrotta, A., Christian, P., Jones, A. O. F., Muralter, F. & Coclite, A. M. Growth Regimes of Poly(perfluorodecyl acrylate) Thin Films by Initiated Chemical Vapor Deposition. *Macromolecules* **51**, 5694–5703 (2018).

123. Christian, P. & Coclite, A. M. Vapor-phase-synthesized fluoroacrylate polymer thin films: Thermal stability and structural properties. *Beilstein J. Nanotechnol.* **8**, 933–942 (2017).

124. Lee, H. S., Kim, H., Lee, J. H. & Kwak, J. B. Fabrication of a Conjugated Fluoropolymer Film Using One-Step iCVD Process and its Mechanical Durability. *Coatings* **9**, 430 (2019).

125. Özpirin, M. & Ebil, Ö. Transparent block copolymer thin films for protection of optical elements via chemical vapor deposition. *Thin Solid Films* **660**, 391–398 (2018).

126. Liu, A., Goktekin, E. & Gleason, K. K. Cross-Linking and Ultrathin Grafted Gradation of Fluorinated Polymers Synthesized via Initiated Chemical Vapor Deposition To Prevent Surface Reconstruction. *Langmuir* **30**, 14189–14194 (2014).

127. Sojoudi, H., Arabnejad, H., Raiyan, A., Shirazi, S. A., McKinley, G. H. & Gleason, K. K. Scalable and durable polymeric icephobic and hydrate-phobic coatings. *Soft Matter* **14**, 3443–3454 (2018).

128. Yun, G. T., Jung, W. Bin, Oh, M. S., Jang, G. M., Baek, J., Kim, N. I., Im, S. G. & Jung, H. T. Springtail-inspired superomniphobic surface with extreme pressure resistance. *Sci. Adv.* **4**, eaat4978 (2018).

129. Vilaró, I., Yagüe, J. L. & Borrós, S. Superhydrophobic Copper Surfaces with Anticorrosion Properties Fabricated by Solventless CVD Methods. *ACS Appl. Mater. Interfaces* **9**, 1057–1065 (2017).

130. Chen, Y., Ye, Y. & Chen, Z. R. Vapor-based synthesis of bilayer anti-corrosion polymer coatings with excellent barrier property and superhydrophobicity. *J. Mater. Sci.* **54**, 5907–5917 (2019).

131. Chen, Z. & Lau, K. K. S. Suppressing Crystallinity by Nanoconfining Polymers Using Initiated Chemical Vapor Deposition. *Macromolecules* **52**, 5183–5191 (2019).

132. Aktas, O. C., Schröder, S., Veziroglu, S., Ghori, M. Z., Haidar, A., Polonskyi, O., Strunskus, T., Gleason, K. & Faupel, F. Superhydrophobic 3D Porous PTFE/TiO 2 Hybrid Structures. *Adv. Mater. Interfaces* **6**, 2–6 (2019).

133. Coclite, A. M. & Gleason, K. K. Global and local planarization of surface roughness by chemical vapor deposition of organosilicon polymer for barrier applications. *J. Appl. Phys.* **111**, 073516 (2012).

134. Ichiki, K., Altemus, B., Gildea, A. & Faguet, J. Feasibility study into the deposition of an organic planarization layer using sequential polymerization initiated chemical vapor deposition. *Thin Solid Films* **635**, 23–26 (2017).

135. Dianat, G., Movsesian, N. & Gupta, M. Process-Structure-Property Relationships for Porous Membranes Formed by Polymerization of Solid Monomer by a Vapor-Phase Initiator. *Macromolecules* **51**, 10297–10303 (2018).

136. Movsesian, N., Tittensor, M., Dianat, G., Gupta, M. & Malmstadt, N. Giant Lipid Vesicle Formation Using Vapor-Deposited Charged Porous Polymers. *Langmuir* **34**, 9025–9035 (2018).

137. De Luna, M. M., Karandikar, P. & Gupta, M. Synthesis of Inorganic/Organic Hybrid Materials via Vapor Deposition onto Liquid Surfaces. *ACS Appl. Nano Mater.* **1**, 6575–6579 (2018).

138. Lee, Y. Il, Jeon, N. J., Kim, B. J., Shim, H., Yang, T. Y., Seok, S. Il, Seo, J. & Im, S. G. A Low-Temperature Thin-Film Encapsulation for Enhanced Stability of a Highly Efficient Perovskite Solar Cell. *Adv. Energy Mater.* **8**, 1701928 (2018).

139. Coclite, A. M. Smart surfaces by initiated chemical vapor deposition. *Surf. Innov.* **1**, 6–14 (2013).

140. Buchberger, A., Peterka, S., Coclite, A. & Bergmann, A. Fast Optical Humidity Sensor Based on Hydrogel Thin Film Expansion for Harsh Environment. *Sensors* **19**, 999 (2019).

141. Unger, K., Resel, R. & Coclite, A. M. Dynamic Studies on the Response to Humidity of Poly (2-hydroxyethyl methacrylate) Hydrogels Produced by Initiated Chemical Vapor Deposition. *Macromol. Chem. Phys.* **217**, 2372–2379 (2016).

142. Christian, P., Tumphart, S., Ehmann, H. M. A., Riegler, H., Coclite, A. M. & Werzer, O. Controlling Indomethacin Release through Vapor-Phase Deposited Hydrogel Films by Adjusting the Cross-linker Density. *Sci. Rep.* **8**, 1–12 (2018).

143. Tufani, A. & Ozaydin Ince, G. Protein gating by vapor deposited Janus membranes. *J. Memb. Sci.* **575**, 126–134 (2019).

144. Muralter, F., Perrotta, A. & Coclite, A. M. Thickness-Dependent Swelling Behavior of Vapor-Deposited Smart Polymer Thin Films. *Macromolecules* **51**, 9692–9699 (2018).

145. Salzmann, P., Perrotta, A. & Coclite, A. M. Different Response Kinetics to Temperature and Water Vapor of Acrylamide Polymers Obtained by Initiated Chemical Vapor Deposition. *ACS Appl. Mater. Interfaces* **10**, 6636–6645 (2018).

146. Muralter, F., Perrotta, A., Werzer, O. & Coclite, A. M. Interlink between Tunable Material Properties and Thermoresponsiveness of Cross-Linked Poly(N - vinylcaprolactam) Thin Films Deposited by Initiated Chemical Vapor Deposition . *Macromolecules* **52**, 6817–6824 (2019).

147. Ghasemi-Mobarakeh, L., Werzer, O., Keimel, R., Kolahreez, D., Hadley, P. & Coclite, A. M. Manipulating drug release from tridimensional porous substrates coated by initiated chemical vapor deposition. *J. Appl. Polym. Sci.* **136**, 47858 (2019).

148. Werzer, O., Tumphart, S., Keimel, R., Christian, P. & Coclite, A. M. Drug release from thin films encapsulated by a temperature-responsive hydrogel. *Soft Matter* **15**, 1853–1859 (2019).

149. Shi, X., Ye, Y., Wang, H., Liu, F. & Wang, Z. Designing pH-Responsive Biodegradable Polymer Coatings for Controlled Drug Release via Vapor-Based Route. *ACS Appl. Mater. Interfaces* **10**, 38449–38458 (2018).

150. Sayin, S., Tufani, A., Emanet, M., Genchi, G. G., Sen, O., Shemshad, S., Ozdemir, E., Ciofani, G. & Ozaydin Ince, G. Electrospun Nanofibers With pH-Responsive Coatings for Control of Release Kinetics. *Front. Bioeng. Biotechnol.* **7**, 309 (2019).

151. O'Shaughnessy, W. S., Murthy, S. K., Edell, D. J. & Gleason, K. K. Stable biopassive insulation synthesized by initiated chemical vapor deposition of poly(1,3,5-trivinyltrimethylcyclotrisiloxane). *Biomacromolecules* **8**, 2564–2570 (2007).

152. Choi, M., Yu, S. J., Choi, Y., Lee, H. R., Lee, E., Lee, E., Lee, Y., Song, J., Son, J. G., Lee, T. G., *et al.* Polymer Thin Film–Induced Tumor Spheroids Acquire Cancer Stem Cell–like Properties. *Cancer Res.* **78**, 6890–6902 (2018).

153. You, J. B., Kim, Y. T., Lee, K. G., Choi, Y., Choi, S., Kim, C. H., Kim, K. H., Chang, S. J., Lee, T. J., Lee, S. J., *et al.* Surface-Modified Mesh Filter for Direct Nucleic Acid Extraction and its Application to Gene Expression Analysis. *Adv. Healthc. Mater.* **6**, 1700642 (2017).

154. Choi, Y., Kim, Y. T., Lee, S. J., Lee, E., Lee, K. G. & Im, S. G. Direct Solvent-Free Modification of the Inner Wall of the Microchip for Rapid DNA Extraction with Enhanced Capturing Efficiency. *Macromol. Res.* (2019). doi:10.1007/s13233-020-8028-x

155. Zhi, B., Song, Q. & Mao, Y. Vapor deposition of polyionic nanocoatings for reduction of microglia adhesion†. *RSC Adv.* **8**, 4779–4785 (2018).

156. Wang, H., Shi, X., Gao, A., Lin, H., Chen, Y., Ye, Y., He, J., Liu, F. & Deng, G. Heparin free coating on PLA membranes for enhanced hemocompatibility via iCVD. *Appl. Surf. Sci.* **433**, 869–878 (2018).

157. Hanak, B. W., Hsieh, C. Y., Donaldson, W., Browd, S. R., Lau, K. K. S. & Shain, W. Reduced cell attachment to poly(2-hydroxyethyl methacrylate)-coated ventricular catheters in vitro. *J. Biomed. Mater. Res. - Part B Appl. Biomater.* **106**, 1268–1279 (2018).

158. Choi, G., Jeong, G. M., Oh, M. S., Joo, M., Im, S. G., Jeong, K. J. & Lee, E. Robust Thin Film Surface with a Selective Antibacterial Property Enabled via a Cross-Linked Ionic Polymer Coating for Infection-Resistant Medical Applications. *ACS Biomater. Sci. Eng.* **4**, 2614–2622 (2018).

159. Youn, Y. H., Lee, S. J., Choi, G. R., Lee, H. R., Lee, D., Heo, D. N., Kim, B. S., Bang, J. B., Hwang, Y. S., Correlo, V. M., *et al.* Simple and facile preparation of recombinant human bone morphogenetic protein-2 immobilized titanium implant via initiated chemical vapor deposition technique to promote osteogenesis for bone tissue engineering application. *Mater. Sci. Eng. C* **100**, 949–958 (2019).

160. Kim, S. H., Yu, S. J., Kim, I., Choi, J., Choi, Y. H., Im, S. G. & Hwang, N. S. A biofunctionalized viral delivery patch for spatially defined transfection. *Chem. Commun.* **55**, 2317–2320 (2019).

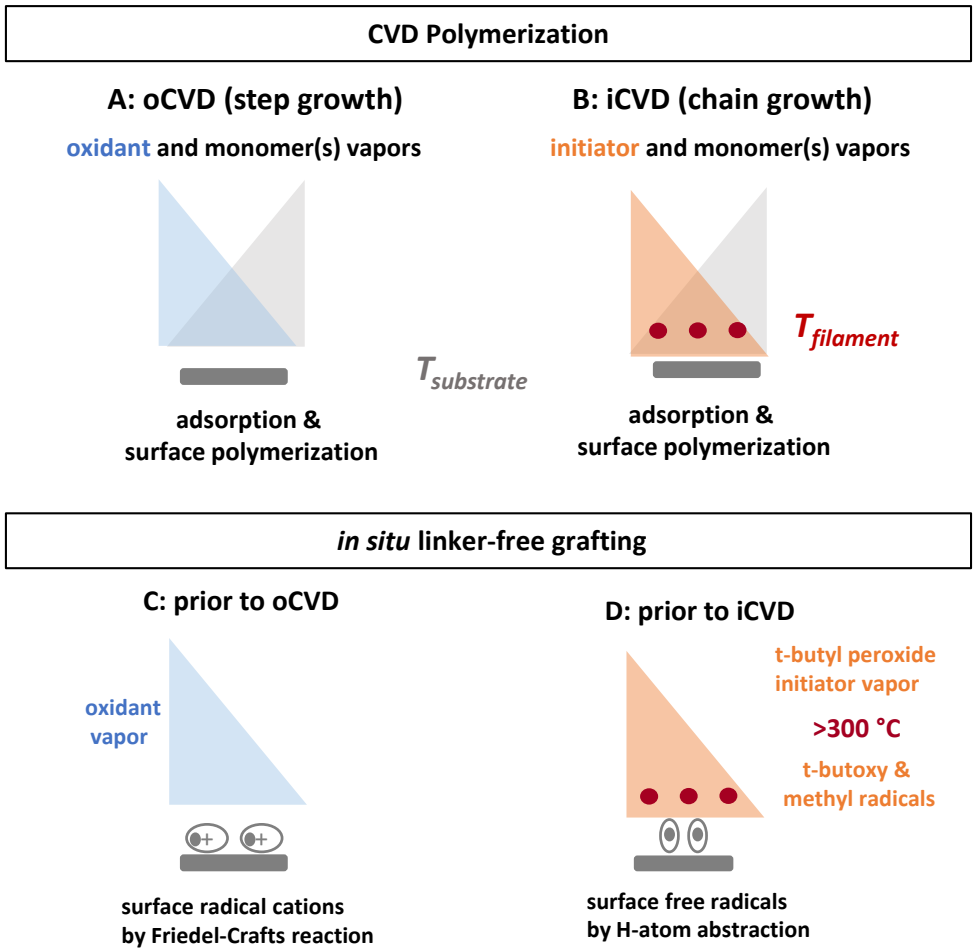

Figure 1: Schematics of a) oCVD and b) iCVD polymerization. Prior to film growth in the same vacuum chamber, exposing the substrate to c) oxidant only or d) initiator only results in situ grafting sites for oCVD and iCVD layers.

(original figure)

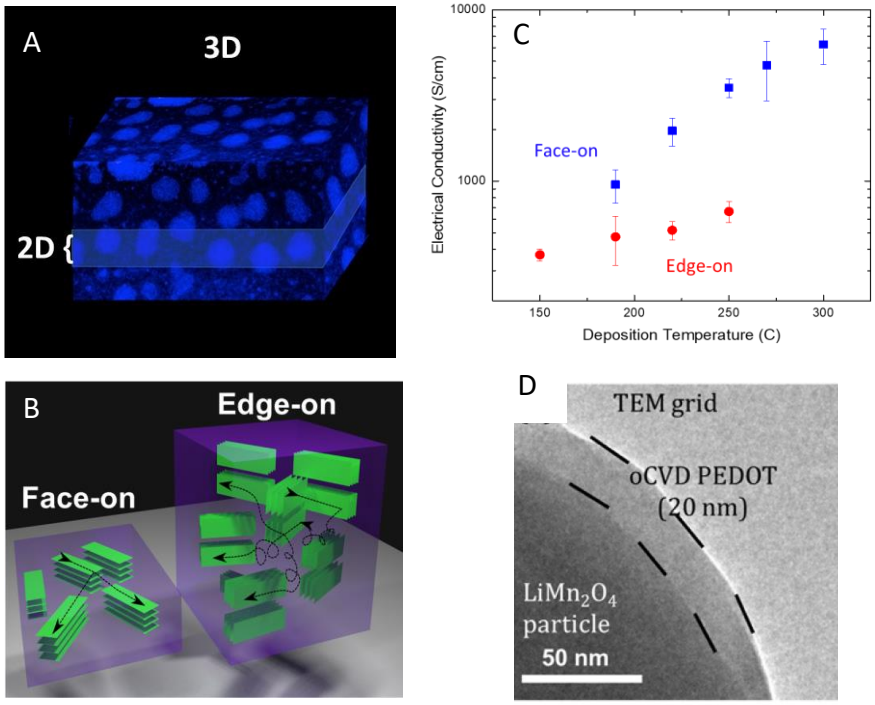

Figure 2: Crystallinity, texture and conformality in oCVD PEDOT. A) Semicrystalline structures with sub-10 nm crystallites revealed by high angle annular dark field scanning transmission electron microscopy. For film thicknesses comparable to the crystallite sizes, electronic conduction becomes 2D. b) The conductive planes of π conjugation (green) oriented either face-on or edge-on with respect to the growth surface. The black lines indicate possible pathways for intercrystallite conduction. c) The in-plane electrical conductivity increases with the surface deposition temperature for two series of films, with higher conductivity observed for the face-on series. d) Transmission electron micrograph of an utrathin and conformal encapsulation of a nanoparticle.

A) Ugur, A., Katmis, F., Li, M., Wu, L., Zhu, Y., Varanasi, K. K. & Gleason, K. K. Low-Dimensional Conduction Mechanisms in Highly Conductive and Transparent Conjugated Polymers. *Adv. Mater.* **27**, 4604–4610 (2015).

B,C) Wang, X., Zhang, X., Sun, L., Lee, D., Lee, S., Wang, M., Zhao, J., Shao-Horn, Y., Dincă, M., Palacios, T., *et al.* High electrical conductivity and carrier mobility in oCVD PEDOT thin films by engineered crystalization and acid treatment. *Sci. Adv.* **4**, 1–10 (2018).

D) Su, L., Smith, P. M., Anand, P. & Reeja-Jayan, B. Surface Engineering of a LiMn 2 O 4 Electrode Using Nanoscale Polymer Thin Films via Chemical Vapor Deposition Polymerization. *ACS Appl. Mater. Interfaces* **10**, 27063–27073 (2018).

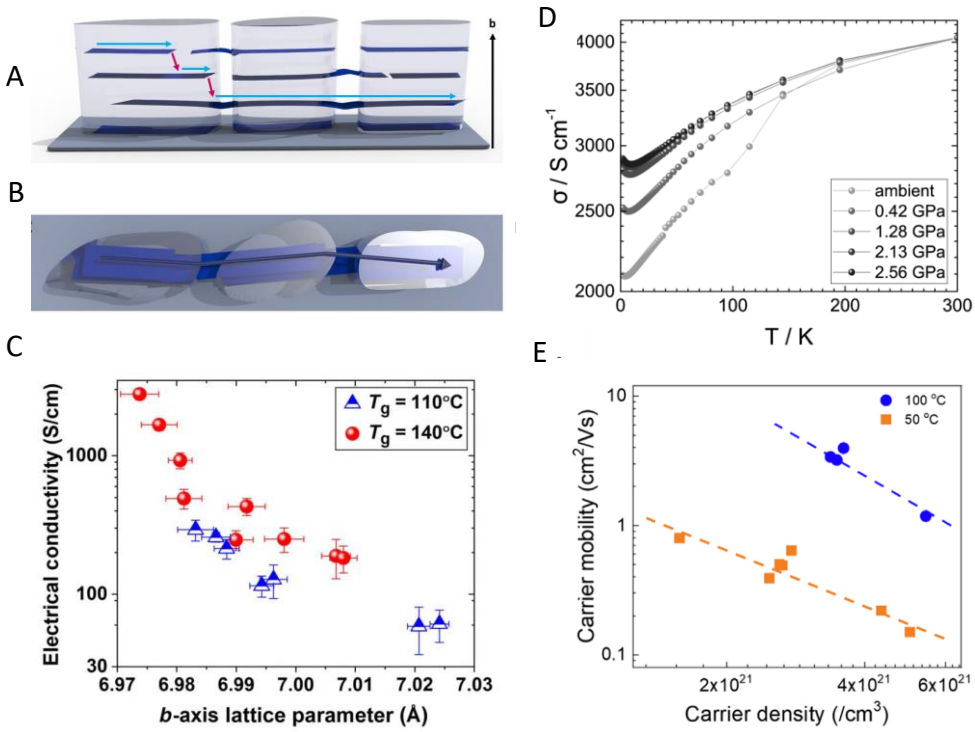

Figure 3: Electrical transport in oCVD PEDOT. a) Schematics of face-on oriented crystallites a) in cross-section, where interchain transport occurs by hopping conduction in domains with ordered π-π stacking and intercrystallite transport is facilitated by bridging chains, and b) top-down, where the result is quasi-1D transport. Measured in-plane electrical conductivity for c) predominate face-on oriented films, grown at either 110 or 140°C, correlates with their lattice parameter for the π-π stacking direction (b-axis) and d) at low measurement temperatures increases with applied external pressure. e) The trade-off between carrier density and mobility in two series of films grown using oxidant sublimed at either 50 or 100 °C.

a,b,c) Gharahcheshmeh, M. H., Tavakoli, M. M. & Gleason, E. F. Tuning , optimization , and perovskite solar cell device integration of ultrathin poly (3 , 4-ethylene dioxythiophene) films via a single-step all-dry process. *Sci. Adv.* 1–13 (2019)

d) Farka, D., Jones, A. O. F., Menon, R., Sariciftci, N. S. & Stadler, P. Metallic conductivity beyond the Mott minimum in PEDOT: Sulphate at low temperatures. *Synth. Met.* **240**, 59–66 (2018).

e) Drewelow, G., Wook Song, H., Jiang, Z. T. & Lee, S. Factors controlling conductivity of PEDOT deposited using oxidative chemical vapor deposition. *Appl. Surf. Sci.* **501**, 144105 (2020).

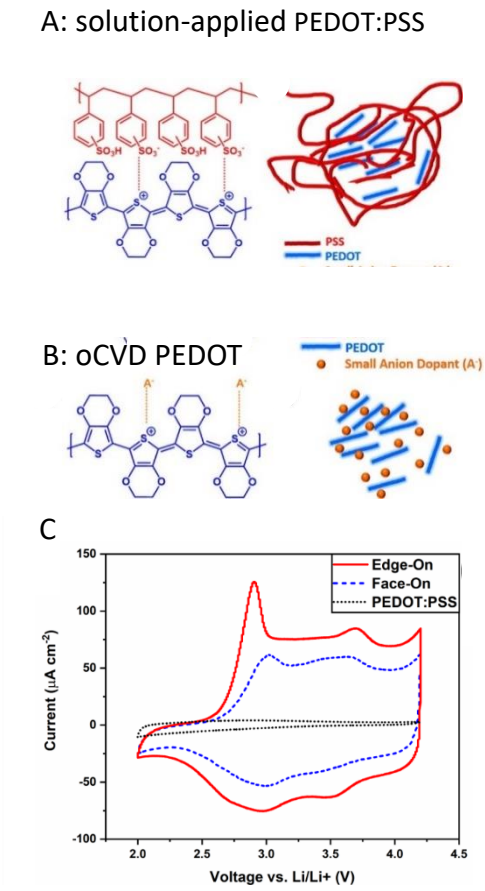

Figure 4: The chemical structure of PEDOT chains doped with a) the macromolecule PSS in solution-applied films and b) small anions, such as Cl^-, in oCVD grown layers. c) The limited mobility of PSS produces corresponding weak electrochemical activity as compared to oCVD PEDOT. For the latter, the influence of crystallite texture is also evident.

4a,b,c Moni, P., Lau, J., Mohr, A. C., Lin, T. C., Tolbert, S. H., Dunn, B. & Gleason, K. K. Growth Temperature and Electrochemical Performance in Vapor-Deposited Poly(3,4-ethylenedioxythiophene) Thin Films for High-Rate Electrochemical Energy Storage. ACS Appl. Energy Mater. 1, 7093–7105 (2018).

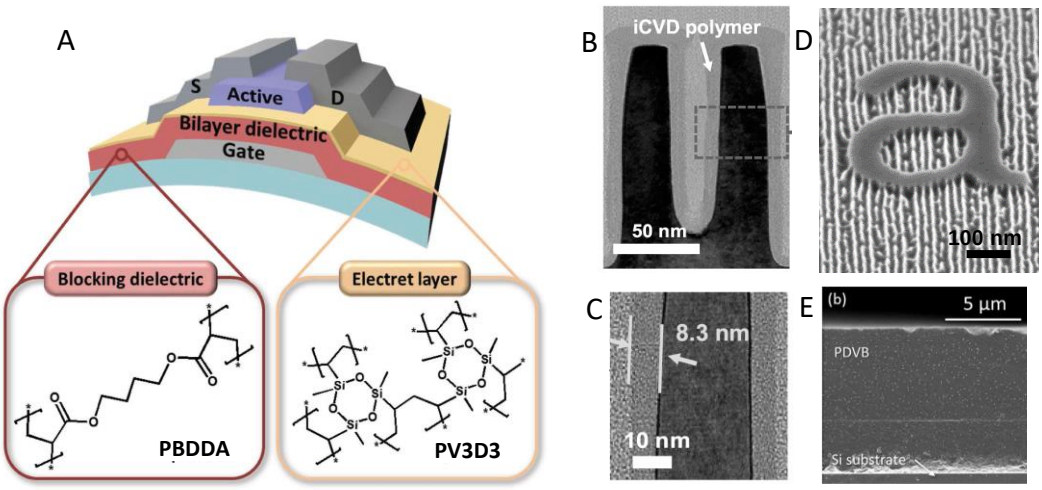

Figure 5. Selected iCVD device and fabrication examples. a) A schematic of a flexible organic thin film transistor for nonvolatile memory utilizing two types of crosslinked iCVD homopolymers. b) Conformal coverage of a dopant-containing iCVD layer 8.3 nm thick over fins in silicon. c) Sub-10 nm line and space patterns in silicon resulted from a directed self-assembly process utilizing ultrathin (<10 nm) iCVD layers grown from the monomer DVB. d) Thick (> 10 μm), low stress iCVD film alsogrown using the DVB monomer.

5a) Pak, K., Choi, J., Lee, C. & Im, S. G. Low-Power, Flexible Nonvolatile Organic Transistor Memory Based on an Ultrathin Bilayer Dielectric Stack. *Adv. Electron. Mater.* **5**, 1–9 (2019).

5b,c) Kim, J. H. *et al. Technical Digest - International Electron Devices Meeting, IEDM* **2018-Decem**, 11.1.1-11.1.4 (2019).

5d) Suh, H. S., Kim, D. H., Moni, P., Xiong, S., Ocola, L. E., Zaluzec, N. J., Gleason, K. K. & Nealey, P. F. Sub-10-nm patterning via directed self-assembly of block copolymer films with a vapour-phase deposited topcoat. *Nat. Nanotechnol.* **12**, 575–581 (2017).

5e) Baxamusa, S. H., Lepro, X., Lee, T., Worthington, M., Ehrmann, P., Laurence, T., Teslich, N., Suresh, A. & Burkey, D. D. Initiated chemical vapor deposition polymers for high peak-power laser targets. *Thin Solid Films* 37–41 (2017).

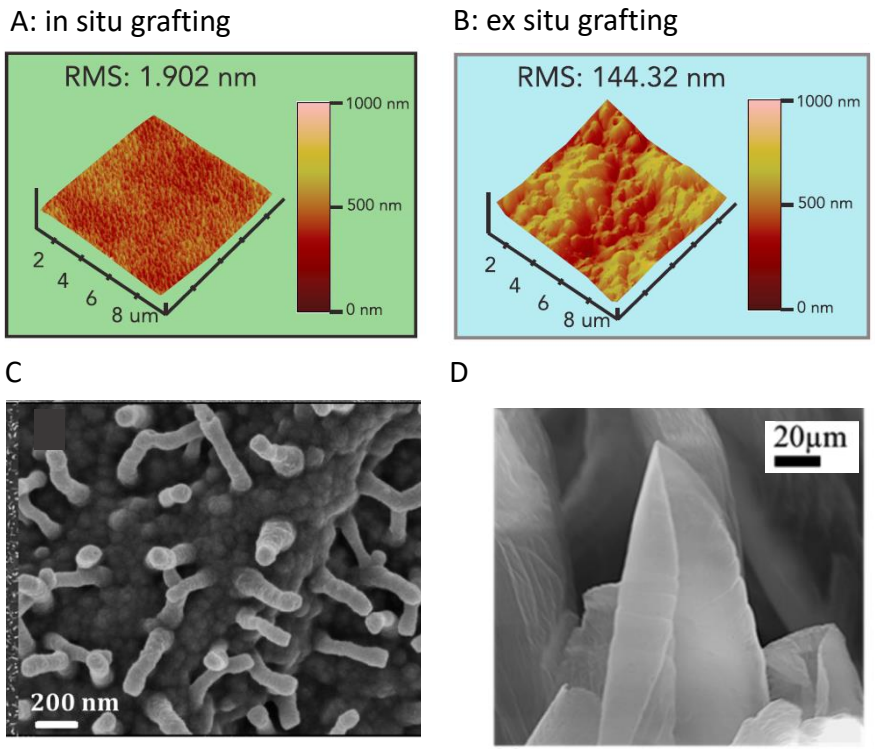

Figure 6. The influence of surface pretreatment on iCVD film morphology Atomic force micrographs of PFDA-based films having (a) in situ and (b) ex situ grafting to a silicon substrate. Electron micrographs of c) PFDA-based nanorods extending from a plasma pretreated copper and d) microstructure formed using a substrate temperature of -20°C, where the MAA monomer solidifies.

6 a,b) Khalil, K. et al. Joule 3, 1377–1388 (2019).

6c) Vilaró, I., et al. ACS Appl. Mater. Interfaces 9, 1057–1065 (2017).

6d) Dianat, G., et al. Macromolecules 51, 10297–10303 (2018).

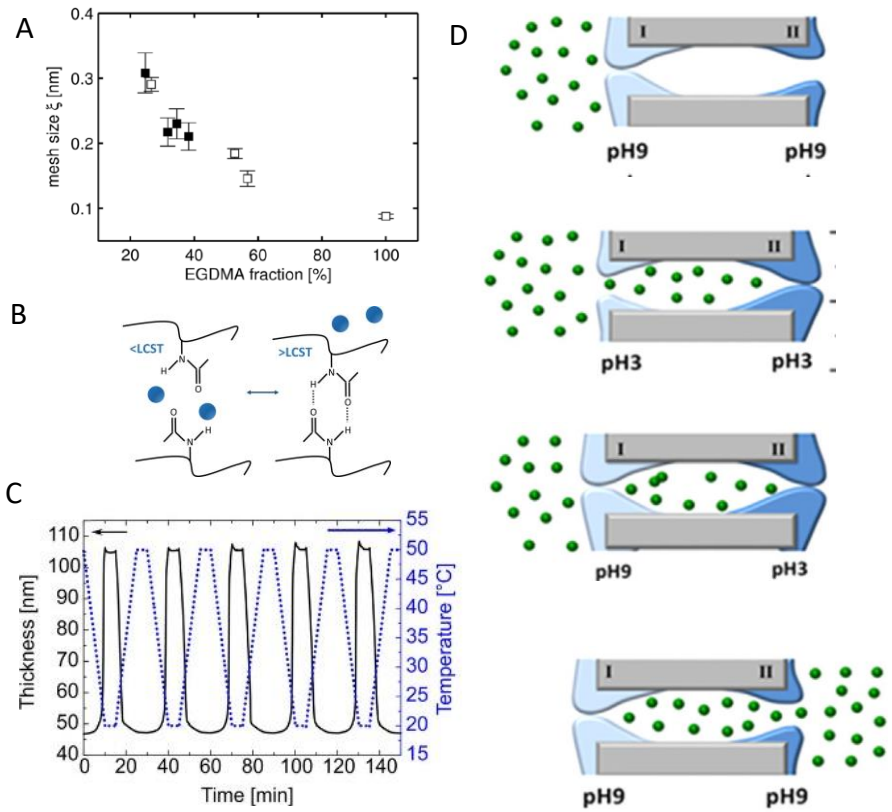

Figure 7: Selected examples of iCVD hydrogels. a) Systematic variation of mesh size for the HEMA copolymer with the crosslinker EGDMA. b) Schematic of the expulsion of water (blue circles) from a thermoresponsive hydrogel upon increasing the temperature above the LCST value. c) Switching the external temperature produces rapid, reversible, and repeatable thickness changes in a nanolayer in NIPAAm copolymer and the crosslinker DEGDVE. c) Schematic of protein (green circles) gating across a membrane pore switched by two different pH responsive iCVD partially conformal layers (light blue and dark blue)

a) Christian, P., Tumphart, S., Ehmann, H. M. A., Riegler, H., Coclite, A. M. & Werzer, O. Controlling Indomethacin Release through Vapor-Phase Deposited Hydrogel Films by Adjusting the Cross-linker Density. *Sci. Rep.* **8**, 1–12 (2018).

b) Muralter, F., Perrotta, A., Werzer, O. & Coclite, A. M. Interlink between Tunable Material Properties and Thermoresponsiveness of Cross-Linked Poly(N -vinylcaprolactam) Thin Films Deposited by Initiated Chemical Vapor Deposition . *Macromolecules* **52**, 6817–6824 (2019).

c) c) Tufani, A. & Ozaydin Ince, G. Protein gating by vapor deposited Janus membranes. *J. Memb. Sci.* **575**, 126–134 (2019).